JOURNAL OF GEOPHYSICAL RESEARCH, VOL. 112, F03023, doi:10.1029/2006JF000739, 2007

Morphology and mechanics of submarine spreading: A case study from the Storegga Slide

Aaron Micallef,[1] Douglas G. Masson,[1] Christian Berndt,[1] and Dorrik A. V. Stow[1]

Received 11 December 2006; revised 22 April 2007; accepted 5 June 2007; published 1 September 2007.

[1] Spreading is a common type of ground failure in subaerial environments. However, this type of mass movement has hardly been documented in submarine settings. In this paper we show that spreading covers at least 25% of the Storegga Slide scar area, a giant submarine slide located offshore mid-Norway. The morphological signature of spreading is a repetitive pattern of ridges and troughs oriented perpendicular to the direction of movement. Two modes of failure can be identified: retrogressive failure of the headwall and slab failure and extension, both involving the breakup of a sediment unit into coherent blocks. These blocks are displaced downslope along planar slip surfaces. Limit equilibrium modeling indicates that loss of support and seismic loading are the main potential triggering mechanisms. The extent of displacement of the spreading sediment is controlled by gravitationally induced stress, angle of internal friction of the sediment, pore pressure escape, and friction. The resulting block movement pattern entails an exponential increase of displacement and thinning of the failing sediment with distance downslope. Sediment properties explain the remaining spatial variation of ridge and trough morphologies associated with spreading.

Citation: Micallef, A., D. G. Masson, C. Berndt, and D. A. V. Stow (2007), Morphology and mechanics of submarine spreading: A case study from the Storegga Slide, *J. Geophys. Res.*, *112*, F03023, doi:10.1029/2006JF000739.

1. Introduction

[2] Spreading is a type of mass movement during which a sediment unit is extended over a deforming mass of softer underlying material [*Dikau et al.*, 1996; *Varnes*, 1978]. Where this occurs, the overlying unit breaks into blocks that move on a gently sloping slip surface. The resulting topography is characterized by a 'ridge and trough' morphology, and the horizontal displacement is in the range of a few meters [e.g., *Kanibir et al.*, 2006]. Other terms, such as gravitational spreading, ridge spreading and lateral spreading, have been used to describe this type of mass movement. Spreading has mainly received coverage in the literature on subaerial geomorphology and geotechnical studies [e.g., *Youd et al.*, 2002], where it has been recognized as the most pervasive type of liquefaction-induced ground failure [*Bartlett and Youd*, 1995]. The occurrence of spreading in submarine environments has hardly been documented, as confirmed by its exclusion from submarine mass movement classification schemes [e.g., *Mulder and Cochonat*, 1996]. Only recently has spreading been reported in the Ormen Lange area of the Storegga Slide, a huge Holocene slide scar located offshore Norway. *Kvalstad et al.* [2005a] and *Gauer et al.* [2005] have commented on its occurrence in the Ormen Lange region and have represented the failure process using energy models and numerical simulations, respectively. Nevertheless, information about the characteristic morphology and distribution of spreading, and understanding of the geological processes responsible for its occurrence, remain scant.

[3] A deeper insight into the submarine spreading process is important for at least two reasons. First, infrastructural work related to natural gas exploitation is currently taking place within the Storegga Slide scar, in the vicinity of areas thought to have been affected by spreading. Thus a better understanding of this process will aid the risk assessment of this potential geohazard. Secondly, the characteristic spreading morphology, in the form of a recurring pattern of ridges and troughs, can be observed in numerous slides around the world, as demonstrated by bathymetric and side-scan sonar images from the Trænadjupet, Nyk, BIG'95 and Eivissa channel slides (Figure 1). A similar morphology has also been identified in the recently discovered Hinlopen Slide [*Vanneste et al.*, 2006], the Grand Banks slope failures [*Piper et al.*, 1999] and in mass movements offshore Mauritania [*Krastel et al.*, 2006]. This shows that spreading is a widespread type of mass movement, and its abundance suggests that it has played an important role in the development of the aforementioned slides. Understanding spreading is therefore a necessary step toward developing more comprehensive models of submarine slope failure.

[4] This paper presents results from a detailed investigation of spreading within the Storegga Slide. The objectives of the study are (1) to characterize the morphological signature of spreading; (2) to understand the mode of failure and controlling factors of spreading, and identify the potential triggers; and (3) to explain the physical boundary

[1]National Oceanography Centre, Southampton, UK.

0148-0227/07/2006JF000739$09.00

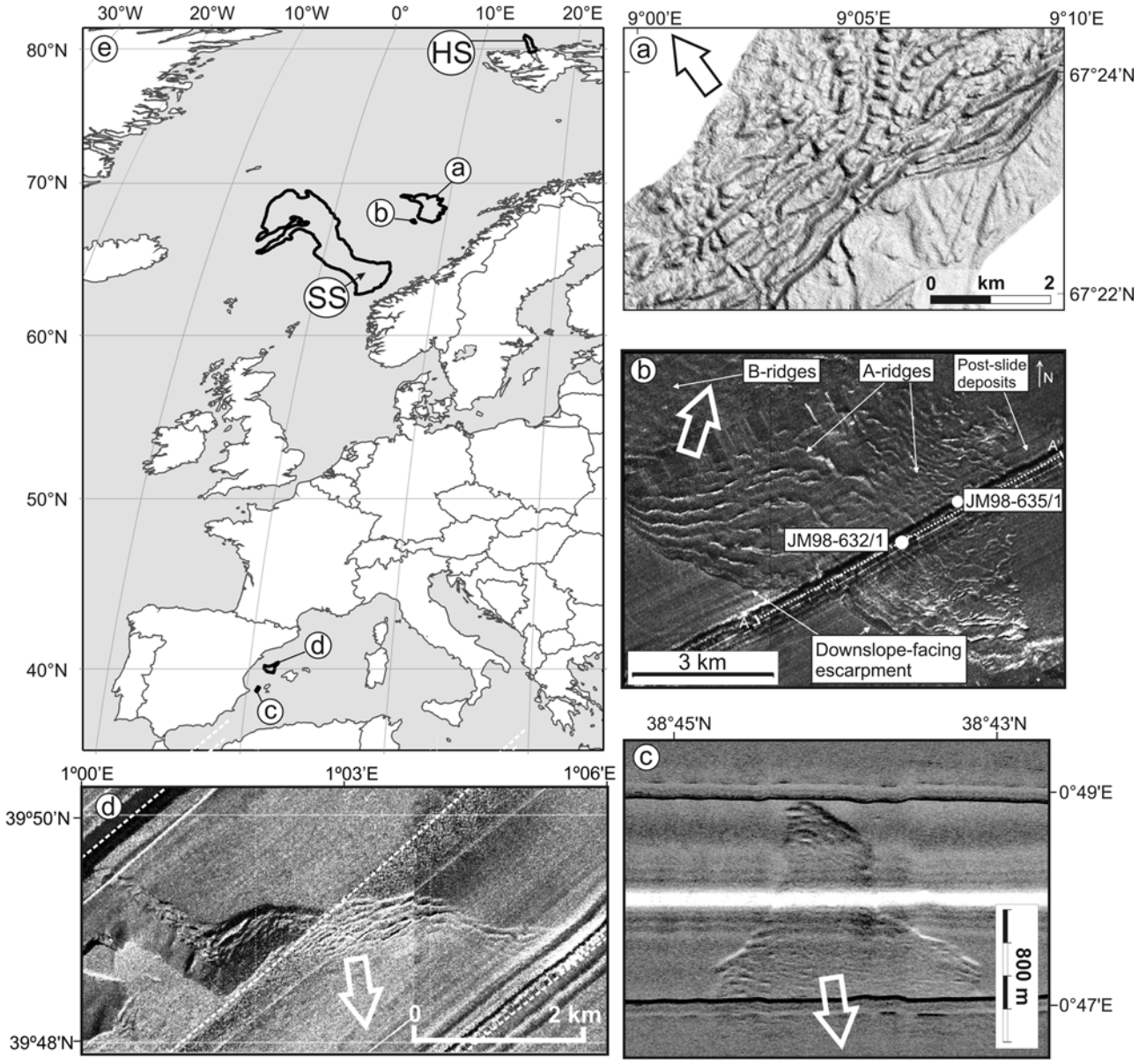

Figure 1. Examples of acoustic imagery of submarine slides that exhibit a ridge and trough morphology: (a) Shaded relief bathymetric map of the Trænadjupet Slide headwall, modified from *Laberg et al.* [2002], reprinted with permission from Elsevier, copyright 2002. (b) TOBI side-scan sonographs of the Nyk Slide headwall, modified from *Lindberg et al.* [2004], reprinted with permission from Elsevier, copyright 2004. (c) MAK-1M sidescan sonar system sonograph across the Nuna Slide headwall scar, modified from *Lastras et al.* [2006, Figure 4], reprinted with kind permission of Springer Science and Business Media. (d) TOBI side-scan sonographs of the headwall of the BIG'95 debris flow, modified from *Lastras et al.* [2003, Figure 2], reprinted with kind permission of Springer Science and Business Media. (e) Map showing locations for Figures 1a–1d in addition to Hinlopen Slide (HS) [*Vanneste et al.*, 2006] and Storegga Slide (SS). The arrows indicate the direction of sediment mobilization.

conditions that control the development of a spread and the associated style of sediment displacement.

2. Regional Setting

[5] The Storegga Slide is located on the mid-Norwegian margin, with the main headwall about 120 km from the Norwegian coastline (Figure 2). The Storegga region has been the site of a number of large-scale mass failures [*Solheim et al.*, 2005], the latest of which was the Storegga Slide, dated at 8100 ± 250 cal. years B.P. [*Haflidason et al.*, 2005]. The repeated sliding activity is due to the influence of climate on sedimentary processes, in particular the alternating deposition of glacial diamictons and ice-proximal

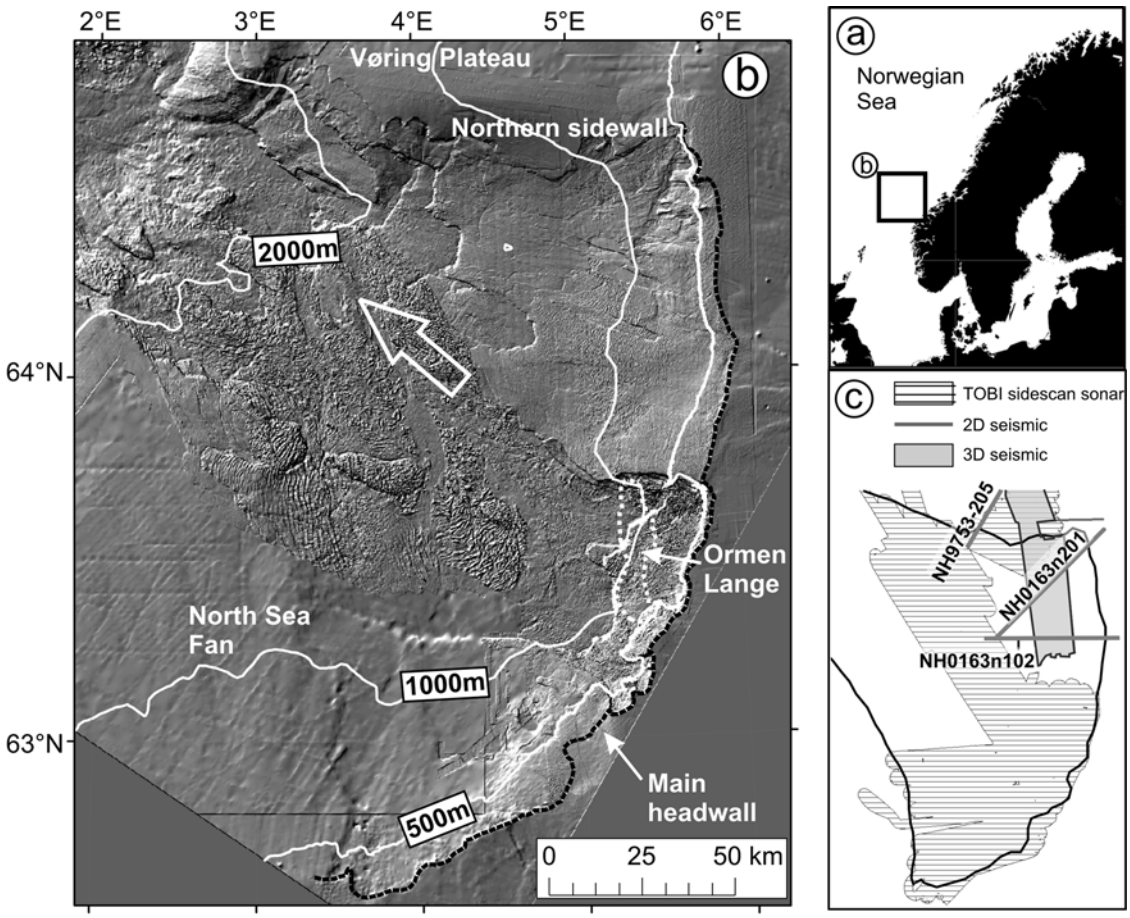

Figure 2. (a) Location of the study area. (b) Shaded relief map of the Storegga Slide scar with bathymetric contours (illumination from NW, 3 times exaggeration). The arrow indicates the direction of sediment mobilization. (c) Spatial coverage of TOBI side-scan sonar and 2-D/3-D seismic data sets.

sediments during glacial maxima, and of fine-grained glacimarine, hemipelagic and contouritic sediments during interglacials [*Berg et al.*, 2005]. The differences in the geotechnical properties of these sediments, coupled with seismicity, rapid sediment deposition and associated high pore pressures, presence of gas hydrates and the regional topography and structural setting, are responsible for more than twenty slope failures during the past 2.6 Ma [*Evans et al.*, 2005; *Solheim et al.*, 2005].

[6] The headwall of the Storegga Slide is coincident with the present-day shelf break. The slide is bound by the Vøring Plateau to the north and the North Sea Fan to the south (Figure 2). With an estimated area of 95,000 km^2 and a volume of 2400–3200 km^3 [*Canals et al.*, 2004], it is one of the largest known submarine slides. The slide scar forms an amphitheater-like depression with a 320 km long main headwall, narrowing downslope to 60 km at a depth of 2000 m. The slide has a depth range of 2700 m and a runout distance of up to 810 km. 90% of the slide scar has a slope gradient of 4° or less, although headwalls reach gradients of 45° and heights of 135 m. According to the interpretation by *Haflidason et al.* [2004], the Storegga Slide has been classified as a complex retrogressive slope failure, consisting of 5 major and 58 smaller events, which have transferred most of the material to the Norwegian Basin.

3. Data and Methods

[7] This study is based on three acoustic data sets (Figure 2c). The first consists of a high-quality multibeam bathymetry data set covering the Storegga Slide from the slide headwall down to a water depth of ca. 2700 m (Figure 2b). The majority of the slide area is covered by data with a horizontal resolution of 25 m or better. The vertical resolution varies from ±10 cm to 2 m at depths of up to 800 m, to ±10 m at 2000 m depths or more. The second data set consists of towed-ocean-bottom-instrument (TOBI) side-scan sonar imagery covering ~60% of the slide scar. The TOBI images have a nominal horizontal resolution of 6 m. The third data set comprises 2-D and 3-D seismic reflection data. High-resolution 2-D lines, located across the main headwall and northern sidewall, have a horizontal resolution of 6.25 m and a vertical resolution of ~2 m. The industry-type 3-D seismic data cover a 2000 km^2 area across the northern sidewall, have a 25 m bin spacing, and ~5 m vertical resolution near the surface.

[8] Previous geomorphological studies of the Storegga Slide have been based on visual interpretation of shaded relief bathymetric maps [e.g., *Haflidason et al.*, 2004; 2005]. Recent studies show that geological interpretation is greatly improved if quantitative techniques are employed. *Micallef et al.* [2007] applied a suite of geomorphometric techniques to the Storegga bathymetry data set to extract quantitative morphological information, which enabled an improved interpretation of shaded relief maps. One of these techniques is called ridge characterization. It involves the automatic extraction of ridge patterns and associated morphological characteristics. These techniques were applied to the Storegga Slide bathymetry data set, and the following ridge and trough characteristic maps were derived (Figure 3): (1) spreading direction, (2) trough depth, (3) ridge length, (4) ridge density, (5) ridge spacing. The grid resolution over which all characteristics were measured was 1 km^2. A geomorphometric map [*Micallef et al.*, 2007] was also generated for the entire Storegga Slide.

4. Results

4.1. Ridge and Trough Morphology

[9] Ridges and troughs at a variety of scales make up one of the most common morphologies observed within the Storegga Slide, particularly in the vicinity of the main headwall (Figures 2 and 4). The ridges and troughs occur in a repetitive parallel to subparallel pattern and are generally aligned parallel to a headwall or escarpment. Close to the headwall, the ridge crests are marked and continuous, with individual ridges having a concave-downslope or linear shape in plan (Figure 4a). Farther downslope, the ridge and trough morphology becomes less distinct, with ridges being more discontinuous. On a few occasions, however, the ridges are unusually high, developing into a convex-downslope pattern in plan (Figure 4a). Areas characterized by ridge and trough morphology are generally wider along slope than downslope. Ridges and troughs can be observed in water depths down to 1500 m. A bathymetric profile across the ridge and trough morphology within the Ormen Lange region shows groups of small and frequent ridges that are located between higher and more infrequent ridges (Figure 4b).

[10] The patterns extracted by the geomorphometric techniques show that ridge and trough characteristics vary spatially across the Storegga Slide (Figure 3). In the majority of cases, zones with the longest ridges coincide with the most widely spaced ridges, the lowest ridge densities and, in most parts, with the shallowest troughs. These patterns are best observed in the northern half of Figures 3b–3d. The ridge direction map (Figure 3a) indicates that the majority of the ridges face a west-northwest direction, with the ridges in the northeast and Ormen Lange area facing in a south-southwest direction.

4.2. Internal Architecture

[11] A seismic dip profile that is perpendicular to the main headwall shows the seismic expression of the ridge and trough morphology (Figures 5 and 6). The seabed reflection is characterized by downslope dipping segments of consistently high amplitude (Figure 6). Below them, a sequence formed by groups of short downslope-dipping high-amplitude reflections, parallel to the surface reflections, are observed, each of them having the same number and pattern of seismic reflections. These groups are separated at regular intervals by upslope dipping segments. A series of four planar, continuous, consistently high-amplitude reflections are observed immediately below this sequence (Figure 6). The ridge crests from a bathymetric profile correspond to the upslope limit of the downslope dipping seabed reflections (Figure 5b). These downslope dipping reflections are thus interpreted as the downslope faces of the ridges. The groups of subseabed reflections are interpreted as blocks that are separated by upslope-dipping interfaces. Using a seismic P wave velocity of 1700 m s^{-1} for the depth conversion, the dip of these interfaces ranges between 24° and 29°, with an average of 25°. Generally the blocks have the shape of a rhomb or trapezium, with top and bottom ~130 m in length. The thickness of the blocks varies between 25 m and 80 m, with a mean of 50 m. Along the entire profile, the base of the blocks corresponds to the topmost continuous high-amplitude reflection of the series of planar reflections. The dip of this reflection, which changes from 1.2° upslope to 0.9° downslope, is lower than the dip of the seabed reflections. Where two blocks are in contact, the seismic reflection of the upslope part of each block is bent downward. The groups of downslope dipping reflectors generally become progressively steeper with distance downslope. The block pattern is best distinguished near the headwall, but becomes less evident downslope. A seismic section downslope of Figure 5b shows that the groups of downslope dipping reflectors, located above the series of planar reflections, are more widely spaced and tilted in comparison to Figure 5b. The seismic reflections are less coherent and the dip of the seabed reflections is more irregular.

[12] The downslope dipping seismic reflectors are interpreted as layers in a stacked sediment package. The blocks of subseabed reflections in the shallower part of the seismic section are interpreted as coherent sediment blocks. The planar continuous reflectors in the deeper part of the seismic section are thought to represent the undeformed sediment unit acting as a slip layer. Layering is preserved in both the upper deformed part and the deeper undeformed part. The blocks are separated by upslope dipping reflectors. These reflectors are interpreted as shear planes and are thought to have formed because of extension because they dip at the angle expected for Mohr-Coulomb failure of these types of sediment [*Kvalstad et al.*, 2005b]. To accommodate this extension, the blocks have translated downslope along a planar slip surface. The surfaces of the blocks are generally steeper than the slip surface, which indicates that the blocks have tilted downslope. During tilting, the upslope top part of each block is exposed, creating a step-like pattern that is responsible for the ridge and trough morphology observed at the surface. The blocks tilt farther downslope with increasing distance from the headwall, which suggests increased extension in this direction. The upslope dipping faces of the ridges are generally steeper than the downslope faces. The downward prolongations of the seismic reflections are considered to be mainly due to diffraction of the seismic energy. The seismic profile and the ridge and trough morphology are considered representative of spreading within the Storegga Slide. Spreading has occurred along

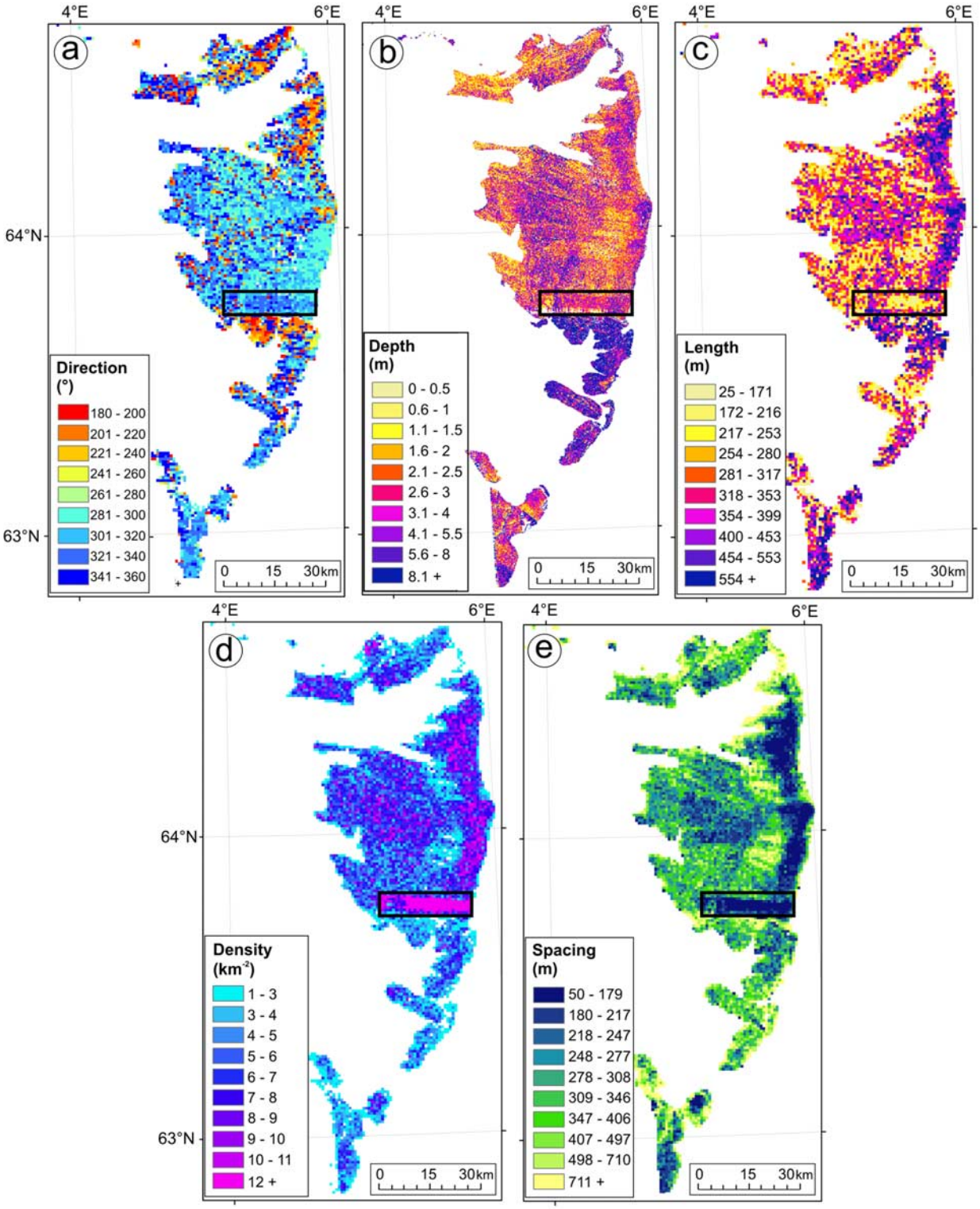

Figure 3. Ridge and trough characteristics maps: (a) Spreading direction (downslope direction perpendicular to the mean orientation of ridges in a grid cell). (b) Trough depth (vertical distance between the base of a trough and the crests of the two adjacent ridges). (c) Ridge length (mean length of individual ridge crests in a grid cell). (d) Ridge density (mean number of individual ridge crests per unit area in a grid cell). (e) Ridge spacing (mean distance between ridge crests in a grid cell). A grid cell has dimensions 1 km $\times$ 1 km. The area covered by the ridge and trough characteristic maps is shown in Figure 7. Note that the resolution of the bathymetry data from the southern part of the Storegga Slide scar is too low to allow calculation of meaningful ridge and trough characteristics. Noise from data merging is indicated by black rectangle.

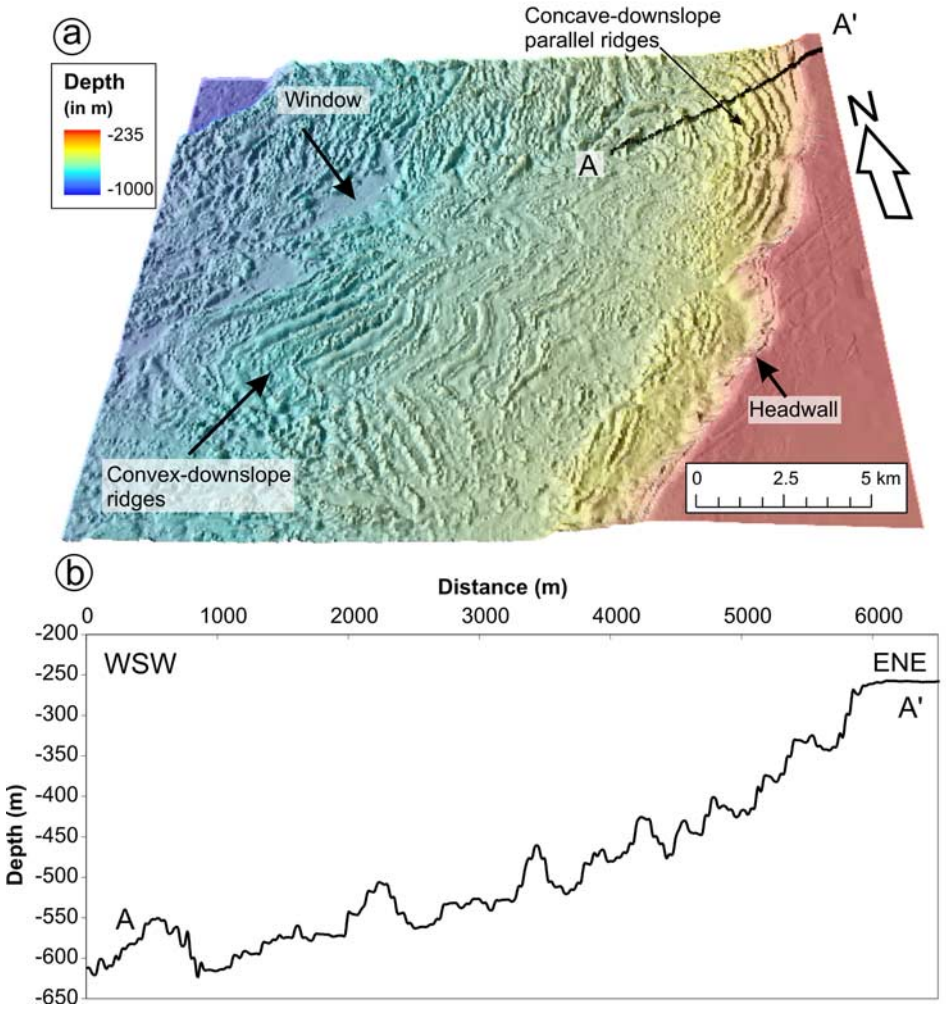

Figure 4. (a) Bathymetric map draped on a 3-D shaded relief image of ridge and trough morphology within the Ormen Lange region of the Storegga Slide. Location is shown in Figure 7. Distinct ridge and trough morphology and windows are noted on the image. A window is defined as a part of the seabed where the slip surface, above which sediment was mobilized during a mass movement, is exposed. (b) Bathymetric profile across ridge and trough morphology close to the main headwall (A-A′). Note that groups of small and frequent ridges are located between higher and more infrequent ridges.

the entire seismic profile (Figure 5a), but the block pattern is best preserved near the headwall (Figure 6a), with increased deformation downslope (Figure 5c).

[13] An alternative interpretation of the seismic section in Figure 6 would be that the blocks were initially formed by Mohr-Coulomb failure with shear planes dipping downslope, and the blocks were subsequently tilted anticlockwise by an angle of $\sim 130°$. Such a process has not been observed in nature so far and would involve significant distortion of the sediment layers within the blocks. Judging from the seismic data (Figures 5 and 6) the internal structure of the blocks is still largely intact and we discard this model as a possible mechanism of spreading.

[14] Our observations are very different from the interpretation of a seismic line proposed for spreading in the Ormen Lange area [*Kvalstad et al.*, 2005a]. These authors interpret almost intact triangular wedges and intermediate distorted rhombs [*Kvalstad et al.*, 2005a, Figure 5]. In their model, shear planes dipping both upslope and downslope delineate the boundaries of the triangular wedges.

4.3. Spatial Distribution of Spreading

[15] Having established that the ridge and trough morphology is indicative of spreading, we investigated its distribution within the Storegga Slide. We combined information from the geomorphometric map with side-scan sonar imagery, seismic data and published geological information to map the spatial distribution of spreading and other mass movements within the Storegga Slide (Figure 7). The mass movements were interpreted on the basis of morphology and internal structure, in accordance with criteria established by *Buma and van Asch* [1996] for spreading and *Mulder and Cochonat* [1996] for submarine mass movements. Only spreads and translational slides are mapped in detail (Figure 7), although topples, rotational slides, debris flows and turbidity currents are known to have occurred [*Bryn et al.*, 2005a; *Haflidason et al.*, 2004]. The current

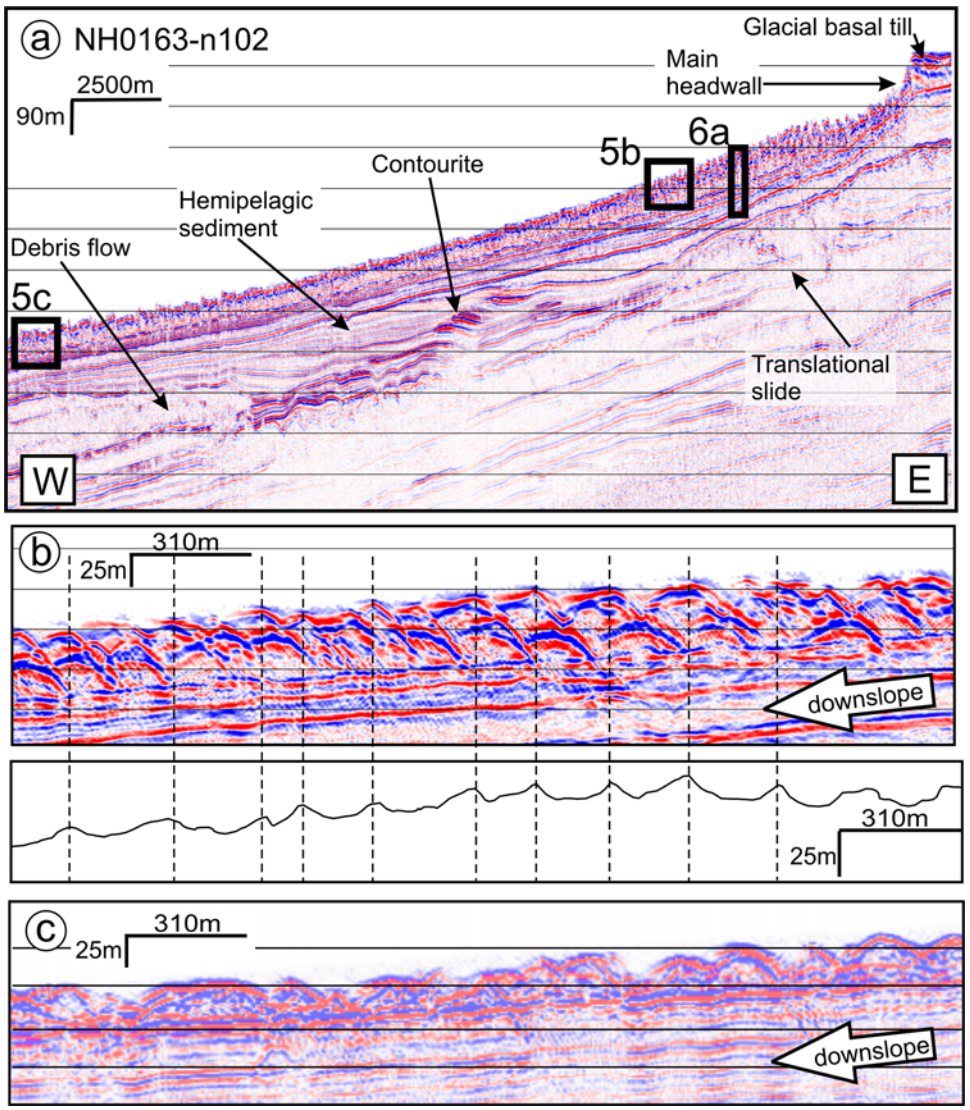

Figure 5. (a) Seismic profile NH0163-n102, located on Figure 7. The seismic signature of the most prominent underlying geological features is indicated. (b) Comparison of a seismic section with the corresponding bathymetric profile extracted from the bathymetry data set. The upslope limit of the downslope dipping surface reflections mainly correspond to the ridge crests in the bathymetric profile, although in some places this is masked by side reflections from adjacent ridges and by other reflection hyperbolae. (c) Enlarged section of part of the seismic section in Figure 5a, illustrating the seismic expression of the ridge and trough morphology downslope of Figure 5b. In comparison to Figure 5b the spreading blocks are characterized by increased deformation and tilting and longer spacing between the blocks. The subhorizontal seismic reflections are still visible within the blocks.

coverage of spreading and complex spreading is 6670 km^2 and 300 km^2, respectively, which add up to ~25% of the total slide scar area. Sediment mobilizations of these types are concentrated along the main slide headwall. Spreading occurs in the northeastern and southern part of the slide scar, whereas complex spreading is mainly found in the central Ormen Lange region. The area affected by translational sliding (426 km^2) is considerably smaller, and is made up of isolated events located at the distal, western limit of spreading in the northeastern part of the slide scar and in the Ormen Lange region. Upslope of these translational slides are numerous windows that expose the underlying slip surface (Figure 7).

4.4. Scales of Spreading

[16] By combining the five ridge and trough characteristics maps (Figure 3) with TOBI side-scan sonar imagery, we are able to identify three zones with different scales of spreading (Figure 8). The morphological characteristics of these zones are listed in Table 1.

4.4.1. Zone 1: Northern and Southern Main Headwall

[17] Zone 1 is by the far the most extensive spreading area. It consists of two disconnected areas, named zones 1a

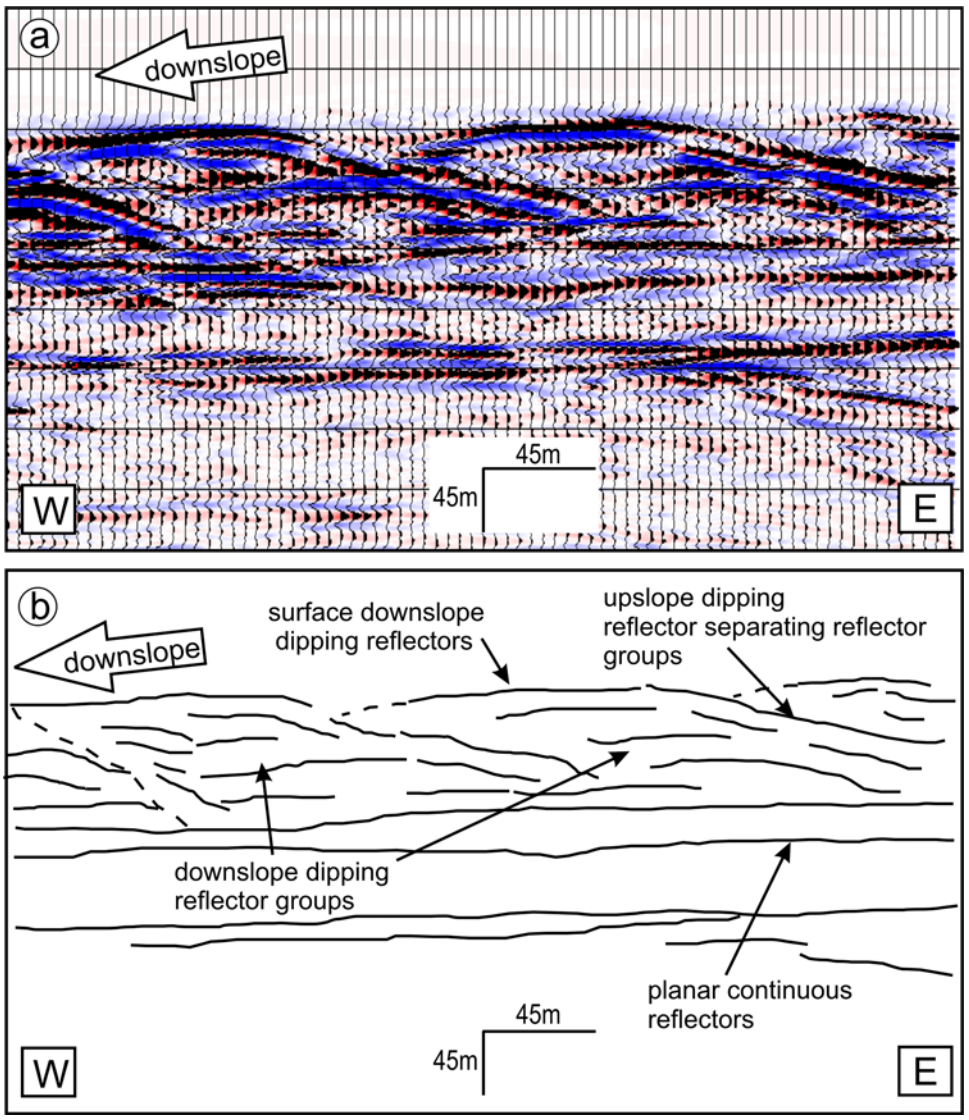

Figure 6. (a) Enlarged section of part of the seismic profile in Figure 5a, with amplitude peaks overlay, illustrating the seismic expression of the ridge and trough morphology at the limit of the data resolution. (b) Labeled interpretation of the seismic section in Figure 6a.

and 1b. Zone 1a has a surface area of 4255 km^2. It is located in the northeastern part of the Storegga Slide and reaches a width of up to 100 km, extending downslope over 50 km. Currently, this spread zone extends from the main headwall, which has a mean height of 50 m, down to the R headwall, although it may originally have extended downslope to the S headwall (Figure 7). In this case most of the downslope section was removed by subsequent mass movement, although some remnants can still be observed in the form of a subtle ridge and trough morphology (Figure 7). The spreading pattern has also been disrupted by debris flows and turbidite pathways in the northeast of zone 1a. Upslope of the R headwall, the ridge and trough pattern is predominantly curved concave downslope or linear. The morphological characteristics of these ridges and troughs are given in Table 1. Three groups of anomalously high, convex-downslope ridges and troughs are located in the middle of the slope and may indicate retardation, halting and possibly compression of the displaced sediment. Although spreading is predominantly an extensional process, some of the ridges and troughs may thus have been formed by localized events of compression. Windows are located downslope of some of these compressional ridges and troughs (Figure 7). In general, the ridges of zone 1a have a gentle downslope face and a steeper upslope face.

[18] Zone 1b comprises an area of 1770 km^2 and ridges are located both upslope and downslope of the O headwall (Figures 7 and 8). High-resolution bathymetry has not been acquired for this region, and interpretations have been based entirely on TOBI side-scan sonar imagery. The ridge and trough morphology and headwall characteristics are very similar to those in the southern half of zone 1a (Table 1). Both linear and curved ridges can be observed (Figure 8b), which are slightly longer than those in zone 1a (Table 1). The ridges are slightly more closely spaced than in zone 1 and the spreading direction is mainly northwest.

[19] Spreading within zone 1 mainly occurs in the shallow O3 sediment subunit (130–30 ka), which consists

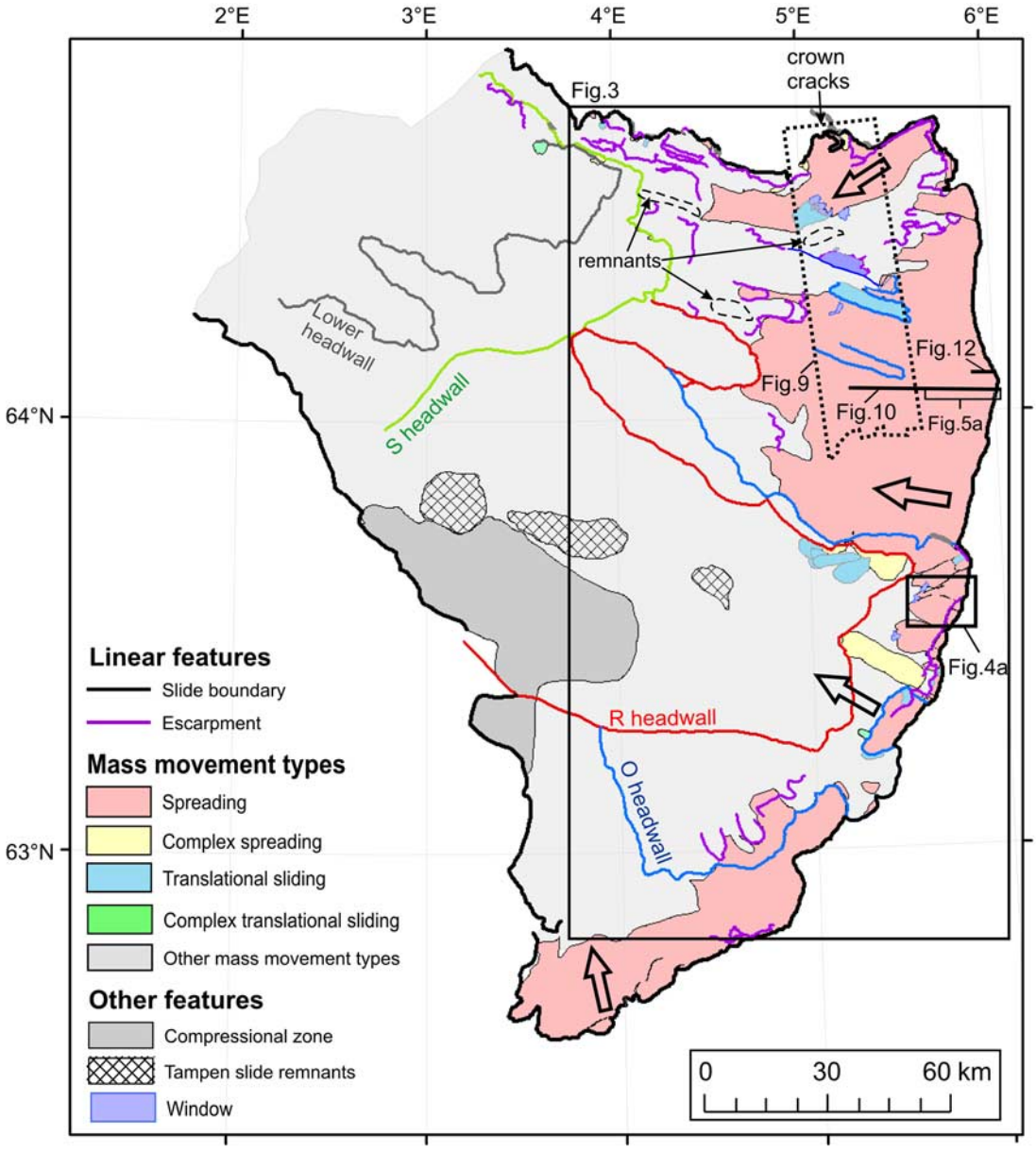

Figure 7. Map of the distribution of mass movement types, headwalls, and other geological features within the Storegga Slide. A complex slope failure is one that was activated as one type of mass movement (as a spread in a complex spread and as a slide in a complex translational slide) but then evolved into a different type of mass movement with distance downslope. Crown cracks indicate zones of incipient failure. The compressional zone in the western part of the slide is due to the impact from large debris flows originating in the Ormen Lange region and is not associated with spreading. Block arrows represent the general direction of mass movement. The names of the headwalls are derived from the sediment units in which failure took place [*Bryn et al.*, 2005a]. Boxes and lines indicate the locations of Figures 3, 4a, 5a, 9, 10, and 12.

of thin stratified deposits of fine-grained normal hemipelagic and glacimarine clays [*Bryn et al.*, 2005a]. In some areas of zone 1, spreading occurs in O1–O2 sediment subunits (30–15 ka), which are made up of basal and deformation till, with subunit O3 acting as the slip surface [*Haflidason et al.*, 2004]. The increase in clay content observed in the lower part of subunit O3 [*Berg et al.*, 2005] may explain the location of the slip surface within this subunit.

4.4.2. Zone 2: Ormen Lange Region

[20] Zone 2 comprises an area of 750 km^2 in the Ormen Lange region between zone 1a and zone 1b, extending from the main slide headwall to the R headwall. Compared to the other zones, the ridges in zone 2 are generally the longest, the widest and the most widely spaced (Figure 8c and Table 1). The troughs are on average almost three times as deep as those in zone 1, whereas the headwall reaches

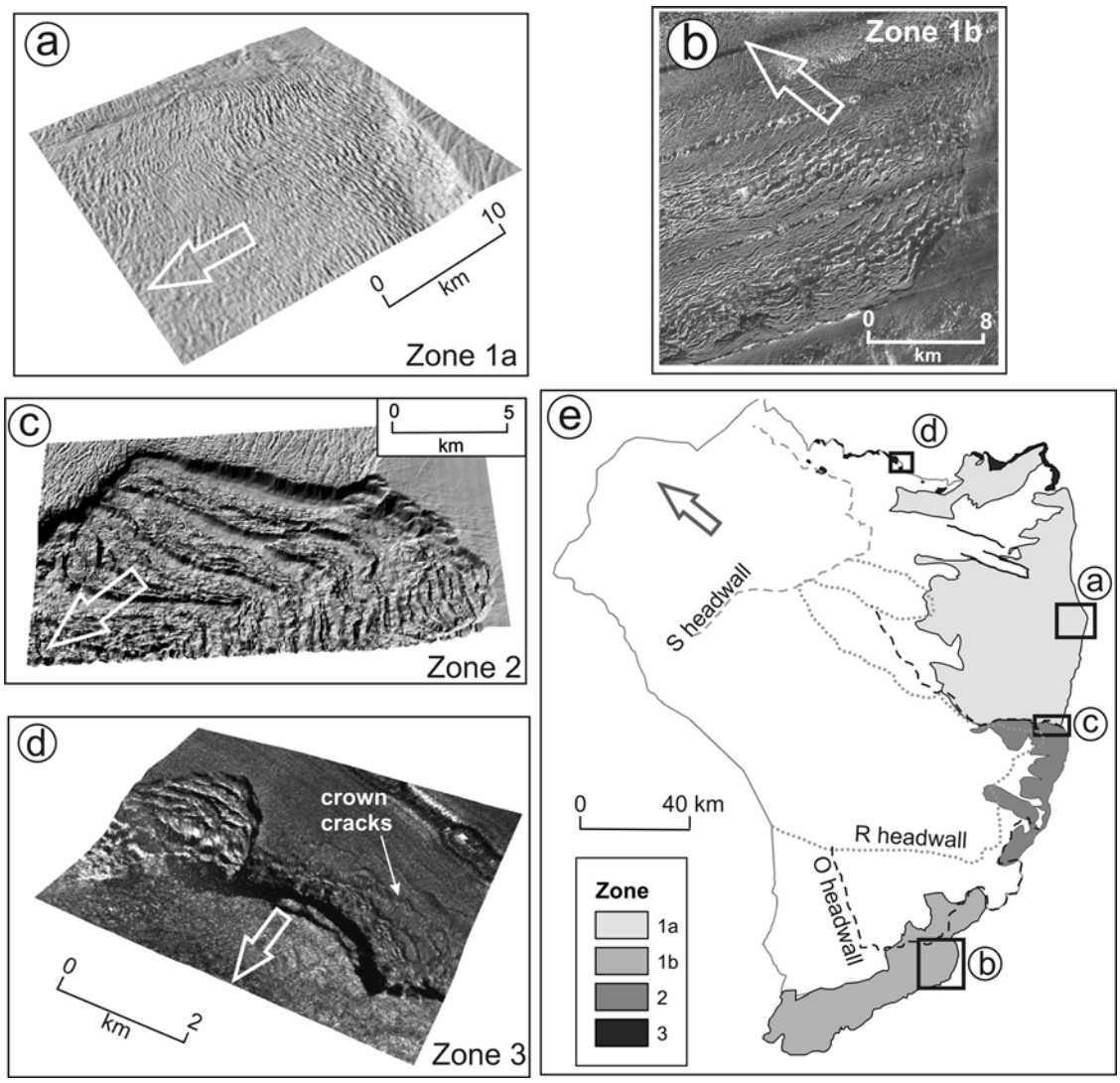

Figure 8. Zonation of spreading within the Storegga Slide: (a) Three-dimensional shaded relief of bathymetry from zone 1a. (b) TOBI side-scan sonar image for zone 1b. (c) Three-dimensional shaded relief image of bathymetry from zone 2. (d) Fusion of TOBI side-scan sonar image with bathymetry in three dimensions for zone 3. (e) Map showing locations for Figures 8a–8d. The arrows indicate the direction of sediment mobilization.

Table 1. Ridge, Trough and Headwall Morphological Characteristics for Zones 1–3[a]

	Zone 1a: Northern Main Headwall	Zone 1b: Southern Main Headwall	Zone 2: Ormen Lange	Zone 3: Northern Sidewall
Area, km^2	4255	1770	750	150
Ridge and trough characteristics				
Mean ridge length, m	334 (±9.3)	345 (±10.1)	397 (±8.1)	292 (±6.1)
Mean trough depth, m	3.1 (±0.5)	3.9 (±0.6)	10.5 (±4.3)	4.9 (±0.8)
Mean ridge spacing, m	287 (±27.4)	261 (±26.2)	361 (±20.2)	213 (±12.8)
Mean spreading direction, deg	293 (±13.1)	316 (±9.5)	272 (±8.6)	235 (±14.1)
Mean ridge density, km^{-2}	6.0 (±0.9)	6.8 (±1.0)	3.8 (±1.7)	8.1 (±0.8)
Headwall Characteristics				
Mean headwall height, m	50 (±4.3)	45 (±2.6)	99 (±18.1)	21 (±2.2)
Range headwall height, m	13–95	21–54	74–135	10–45
Mean slope gradient, deg	4.83 (±0.8)	6.48 (±1.4)	14.5 (±7.1)	4.05 (±0.5)
Maximum slope gradient, deg	23	23	32.5	21

[a]Standard error for the listed means is also shown.

heights of up to 135 m, with a mean slope gradient of 14.5°. The mean direction of spreading is westward, although the ridges have many orientations. Where the spreads collapse over an escarpment, the ridge and trough morphology is generally preserved. The headwall is higher in the southern part of zone 2 and the adjacent ridges are linear, whereas concave-downslope spreading ridges merge with a lower headwall in the northern part. Shear zones in the ridge and trough pattern, caused by different events or rates of spreading, can be observed in this zone. Remnants of zone 1a spreading ridges can be distinguished on top of ridges from zone 2, indicating that spreading in zone 2 postdates events in zone 1a (Figure 8c). In contrast to zone 1, the downslope face of the ridges in zone 2 is generally steeper than the upslope face. Numerous windows have been identified in this zone (Figures 4a and 7). Pronounced, long convex-downslope ridges and troughs are located upslope of these features. Spreading in zone 2 mainly occurs in the deep and thick O4–O7 sediment subunits (200–130 ka), consisting of glacial till and debris flow deposits [*Berg et al.*, 2005]. The glacial to normal hemipelagic clays of subunit R2 (330–200 ka) make up the slip surface [*Kvalstad et al.*, 2005a].

4.4.3. Zone 3: Northern Sidewall

[21] Zone 3 has an area of 150 km^2. It extends upslope from the northern sidewall and the main Storegga Slide headwall. It consists of a concentration of small spreads on the top of the northern sidewall and just above the headwall of zone 1a. The spreading areas are elongated, narrow and found on top of escarpments created by larger failures. Where the spread zone extends farther upslope, it is arcuate in plan, with subparallel ridges and troughs that are concave downslope. Numerous zones of incipient failure exhibiting systems of crown cracks occur adjacent to or upslope of the spreads (Figure 8d). The spacing of the crown cracks is about 100 m. The fact that the shape of these open fractures is similar to that of the ridges and troughs to the west implies that the latter have formed by extension. Additionally, within zone 3, iceberg plough marks can be seen running from the ridges and troughs to the undisrupted slope, indicating limited extensional displacement of the ridges since the Last Glacial Maximum (LGM). Zone 3 is characterized by the lowest headwall, shortest ridges, shortest ridge spacing and highest ridge density. The mean trough depth is 4.88 m, slightly deeper than for zones 1a and 1b. The ridges of zone 3 have a steep downslope face and a gentler upslope face. Spreading in zone 3 takes place in the uppermost sediment subunits (O1–O2).

4.5. Thickness of Failed Sediment and Slip Surface Characteristics

4.5.1. Sediment Thickness and Associated Ridge and Trough Morphology

[22] The 3-D seismic data were used to interpret the slip surface of the spreading within zone 1a and to generate an isopach map for the sediment above this slip surface (Figure 9a). Time-to-depth conversion of the seismic data was carried out using a seismic P wave velocity of 1700 m s^{-1} for the sediment. For zone 1a, the range of thicknesses is 22 to 44 m. In general, the thickness of the sediment affected by spreading in zone 1a decreases downslope from east to west. Given the amount of vertical strain that appears to have occurred with distance of movement downslope, we infer that the deformation of the spreading sediment is not entirely brittle, but a significant part of the sediment has undergone quasi-plastic deformation. When compared to the ridge and trough characteristics maps in this area of the Storegga Slide (Figure 3), the thinnest parts of the section affected by spreading coincide with the deepest troughs, shortest ridge spacing, highest ridge density and decreasing ridge length.

[23] The interpreted seabed and slip surface of the spread along a high-resolution 2-D seismic line shows that the calculated thickness of the spreading gradually decreases with distance downslope (Figure 10a). The corresponding ridge and trough characteristics at the surface of the spread also change systematically downslope (Figure 10b), and match the relations observed in the 3-D seismic data. Trough depth shows a general increase from 1.5 m near the headwall to 5.5 m toward the toe. The ridge length peaks at the centre of the slope with 410 m, and decreases both upslope toward the headwall and downslope toward the distal limit. Ridge density increases away from the headwall, whereas the ridge spacing decreases downslope. These trends in ridge and trough morphological characteristics indicate that the spreading blocks are undergoing progressive fragmentation, deformation and tilting with distance downslope.

[24] In both the 2-D and 3-D seismic data sets, the thickness of the spread layer is thinner than what could be assumed for the preslide thickness, which at the headwall is ~80 m (Figures 9a and 10a). Both data sets show a clear reduction of sediment thickness with distance downslope and there are no trends of increasing sediment thickness, and possibly compression. These indicate that the spreading process is mainly extensional, although part of the reduction of sediment thickness with distance downslope may be attributed to inherent stratigraphical variation [*Berg et al.*, 2005].

4.5.2. Slip Surface Morphology

[25] The shaded relief image of the interpreted slip surface exhibits the same general morphology as the seabed, but with a lower mean slope gradient of 0.5° (Figure 9b). The arrows in Figure 9b represent the spreading direction of the ridges, which is generally perpendicular to the depth contours of the interpreted slip surface. This indicates that the spreading direction is determined by the aspect of the slip surface. This is also confirmed by the high correlation (R^2 = 0.91) between spreading direction of the ridges and the slope aspect of the slip surface for the entire 3-D block using 1 km^2 grids.

4.6. Displacement Associated With Spreading

[26] Interblock displacement is the increase in the distance between identical reference points on two successive blocks when spreading occurs. Figure 11a shows a cross section of two blocks before spreading occurs, with *o* being the distance between the top upslope corners of the two blocks, here considered as the two reference points. Figure 11b shows the displaced and tilted blocks after spreading has occurred, with *n* representing the new distance between the two reference points. *h* is the sum of the vertical distances that the downslope corner of the upslope block and the upslope corner of the downslope

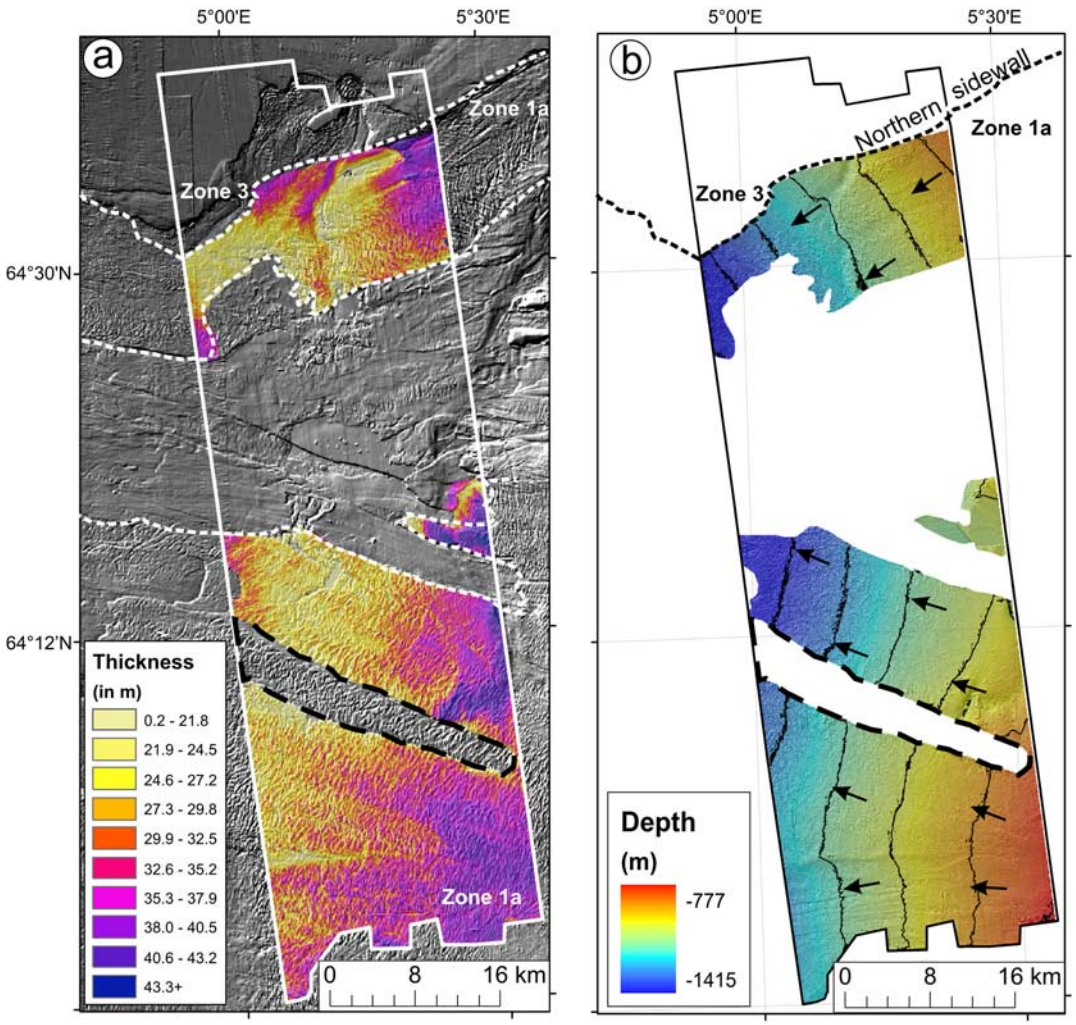

Figure 9. (a) Isopach map of zone 1a spread. The solid white line indicates the limits of the 3-D seismic data, whereas the dotted white line shows the boundary of the spreading zone 1a. (b) Shaded relief map and contours (at 100 m intervals) of the interpreted slip surface. The arrows indicate the general spreading direction of the overlying ridges. The maps are derived from the 3-D seismic data set, the location of which is shown in Figure 7. Since the error associated to the 3-D seismic data is quite high in relation to the spread thickness, the values in Figures 9a and 9b are not absolute. However, these values do allow us to understand the relative integral variation of thickness and elevation. The gaps in the data observed in the southern central parts of Figures 9a and 9b (outlined by a dashed black line) are due to the fact that the slip surface, above which spreading has occurred, is deeper in this region.

block have moved, and α represents the angle of tilting. The interblock displacement can therefore be calculated as:

$$\text{interblock displacement} = n - o = n - (h/\sin\alpha) \qquad (1)$$

Since n and h can be measured from the bathymetry, and α from the seismic profile, the interblock displacement can be calculated.

[27] Being able to estimate the interblock displacement for successive pairs of blocks allows us to calculate the cumulative displacement of each block from its original position. This is achieved by adding up the values of the interblock displacement upslope of a block. The approach was tested on a 5 km length of spread located downslope of the main Storegga headwall, where the widths of the blocks are almost identical. The resulting graph for the displacement of successive blocks along the profile shows a gentle exponential decay of displacement with distance upslope (Figure 12). This decay is an indication that the tilting of the blocks decreases progressively upslope. The exponential decay in displacement is composed of successive clusters of blocks that also exhibit an exponential decay in displacement with distance upslope. The extension factor calculated for the section of the slope under consideration is 1.10. This value indicates that a sediment unit undergoing spreading is extended by ~10% of its original length. This should be considered as a minimum estimate because subseismic-scale deformation is not being taken into con-

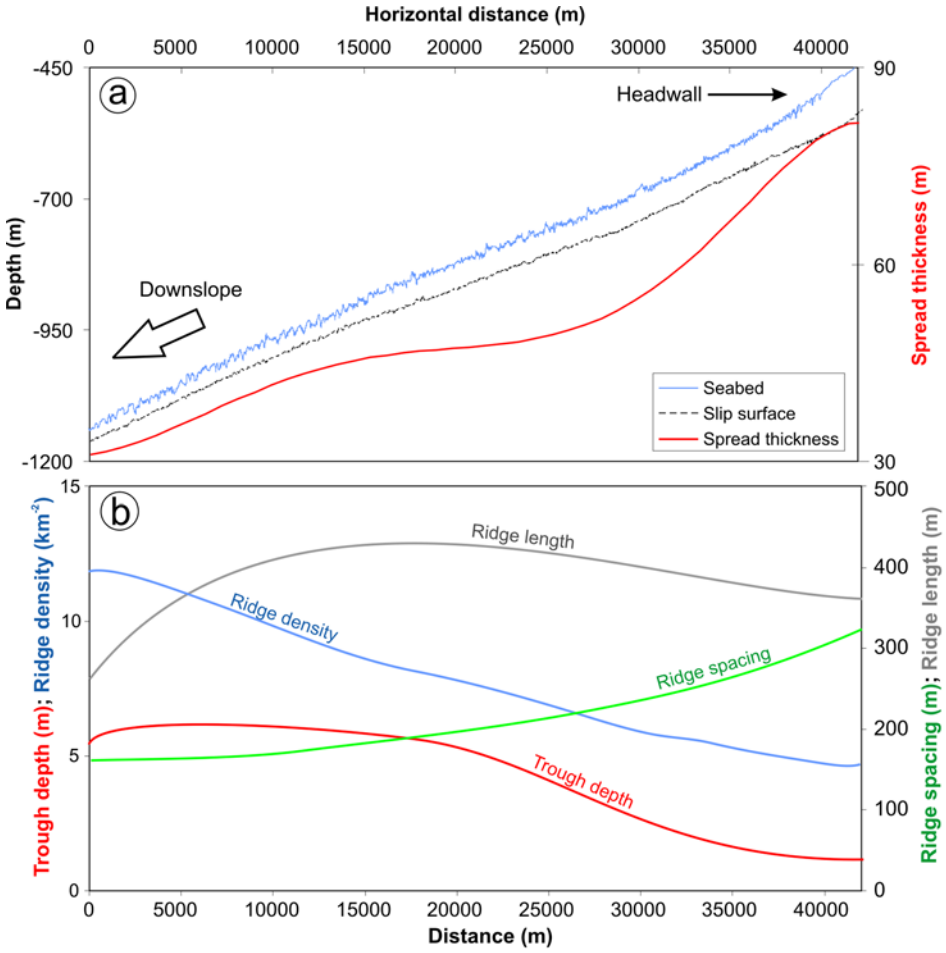

Figure 10. (a) Cross-sectional profile across a spread in seismic line NH0163-n102, showing the interpreted seabed and slip surface. The calculated thickness of the spread, which is also shown, varies from 80 m near the headwall to 32 m farther downslope. (b) Polynomial trend lines fitted to the corresponding variation of ridge and trough characteristics across the surface of the spread in Figure 10a. The location of line NH0163-n102 is shown in Figure 7.

sideration and can accommodate considerable extension [*Marrett and Allmendinger*, 1992].

5. Discussion

5.1. Mode of Failure

[28] Two modes of failure may be proposed for spreading within the Storegga Slide: (1) In model 1, spreading develops retrogressively along the slip surface by the repeated failure of the headwall. The failure propagates upslope via the fracturing of the sediment into a number of coherent blocks. The blocks progressively undergo translation and disintegration. (2) In model 2 the material above the slip layer behaves as a thin coherent slab that is extended downslope by gravity, and having drag forces resisting the movement at the base. The resultant downslope stress to which the slab is subjected is higher downslope than upslope, generating the necessary tension to break the slab up.

[29] Model 1 is essentially the model suggested by *Kvalstad et al.* [2005a] for mass movements within the Ormen Lange region (our zone 2). Unloading of the headwall at the base of the slope results in the formation of shear planes that define a triangular failing sediment block accelerating downslope. This is pushed forward along the slip surface by an inverted triangular wedge that undergoes internal distortion. The process is assisted by pore pressure development in the toe area because of shear-induced contraction of the marine clay [*Kvalstad et al.*, 2005a]. For this model to be applicable the fracturing between the blocks should obey the Mohr-Coulomb failure criterion and the shear planes should be downslope dipping. The first condition is observed in our seismic data from zone 1, whereas the second is not (Figure 6). Furthermore, the downslope faces of the ridges formed by model 1 should be steeper than the upslope faces (as in Figure 7 of *Kvalstad et al.* [2005a]). This is seen within zones 2 and 3 of spreading, but not in zone 1. This means that model 1 can only be applied to spreading in zones 2 and 3, but that the mode of failure in zone 1 must be different.

[30] In model 2, gravitational forces act on a thin and long slab of semiconsolidated material possibly underlain by a failure surface or a liquefied weak layer. Material under tension in this way can be expected to rupture in a closely spaced series of coherent blocks, resulting in ridges and

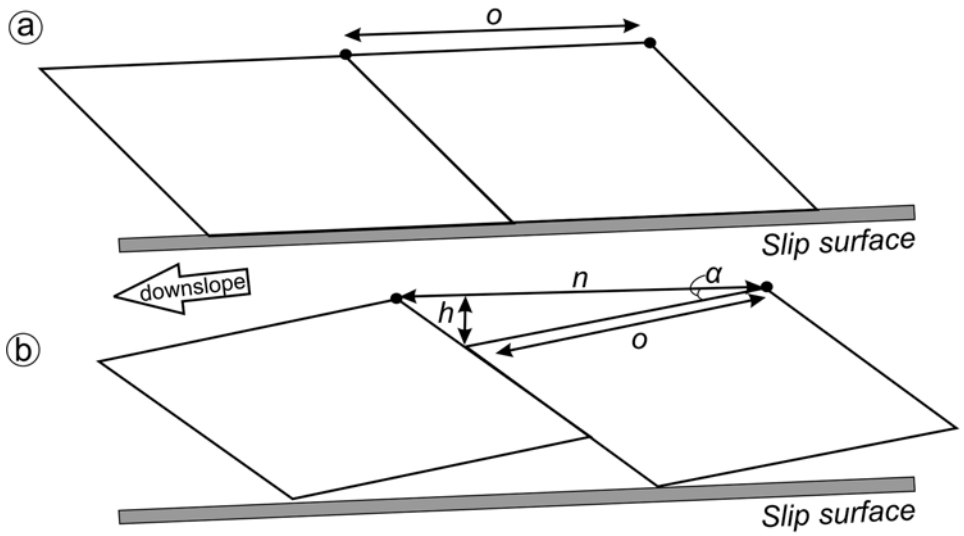

Figure 11. Schematic representation of two blocks within a spread (a) before failure and (b) after failure. Here o is the initial distance between two reference points, n is the final distance between the two reference points, h is the sum of the vertical distances moves by the two reference points, and α is the angle of tilting of the block. Reference points are marked by a circle. This representation does not take into account the deformation that occurs at the base of the slope.

troughs at the surface (similar to ''boudinage'' occurring on the flanks of folds). This model is put forward as the mechanism responsible for spreading in zone 1, where the failed sediment was thin relative to the distance across which failure can be observed (Figures 5 and 6). The upslope dip of the internal extension faults within the slab is interpreted as an indication that the extensional forces acting on the slab decreased upslope and the frictional drag on the base of the slab increased upslope. The latter may have been due to a decrease in excess pore pressure in the failing layer upslope (away from the source of the overall retrogressive Storegga Slide, as suggested by *Strout and*

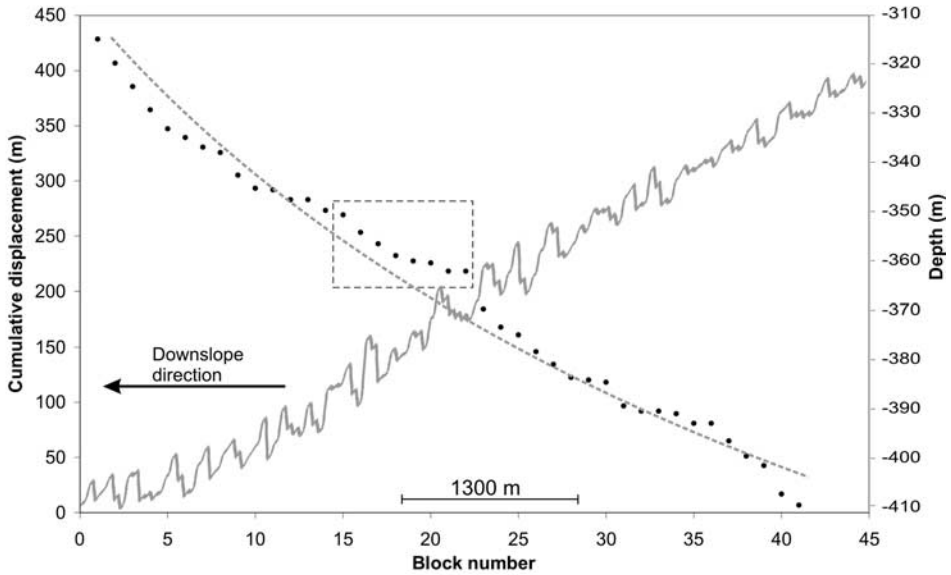

Figure 12. Plots of the bathymetric profile showing the ridge and trough morphology (solid shaded line, location shown in Figure 7) and the estimated cumulative displacement of the associated blocks versus block number (circles). Block number refers to the order in which the blocks are mobilized. The dotted shaded curve is the line of best fit and is indicative of a gentle exponential decay of displacement with distance upslope. A subgroup of blocks showing exponential decay of displacement is enclosed in a dotted shaded square.

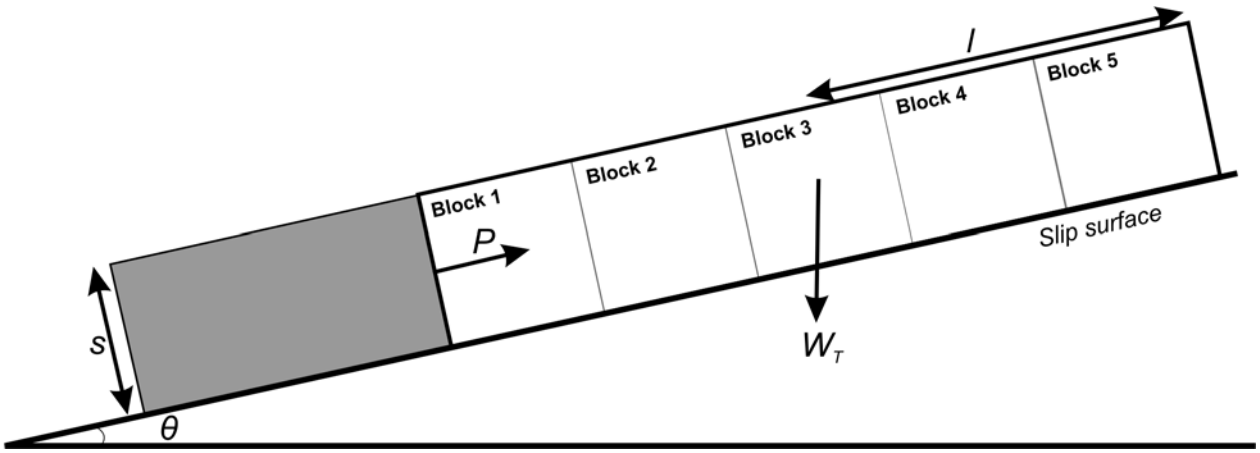

Figure 13. Illustration of the mechanical model, showing some of the static forces that act on a sediment slab prior to failure as well as the dimensional attributes. The dark shaded block at the downslope part represents the part of the slope that will fail, activating spreading in the sediment slab enclosed by the bold black border.

Tjelta [2005]). Alternatively, the physical character or thickness of the failing layer (believed to be contouritic glaciomarine sediments [*Berg et al.*, 2005]) may have varied with water depth, as is seen in present-day distribution of post-Storegga Slide sediments [*Bryn et al.*, 2005b]. In model 2, failure can potentially start from anywhere along the slope. In this model, the formation of shear planes is expected to obey the Mohr-Coulomb failure criterion and the upslope faces of the ridges should be steeper than the downslope faces. Both conditions are observed in spreading within zone 1 (Figure 6).

5.2. Modeling Spreading

[31] Models of spreading have previously been used to determine horizontal ground displacements. In subaerial settings, modeling has been carried out in three main ways: (1) empirical methods [e.g., *Youd et al.*, 2002]; (2) simplified analytical models [e.g., *Dobry and Baziar*, 1992]; and (3) finite element methods [e.g., *Kanibir et al.*, 2006]. Modeling of submarine spreading is limited to a numerical model based on the energy approach [*Kvalstad et al.*, 2005a] and the combination of computational fluid dynamics with strain-softening material models [*Gauer et al.*, 2005]. We model submarine spreading using limit equilibrium and mechanical models that are applicable to the two modes of failure discussed in section 5.1. In this way we can identify the triggers of a spread, model the pattern of block displacement, and understand which factors control the spreading process.

5.2.1. Limit Equilibrium Model

[32] We consider a thin slab of sediment resting on a planar slip surface, which is initially supported by another slab of sediment downslope. The static forces acting on the upslope slab are illustrated in Figure 13. To simplify calculations, the slab consists of a number of adjacent and equidimensional blocks. The static forces acting on each block can be divided into driving forces:

$$\text{driving forces} = \sin\theta[W_T] \tag{2}$$

and resisting forces [*Terzaghi and Peck*, 1967]:

$$\text{resisting forces} = \tan\phi[W_T(\cos\theta) - u] + c + P \tag{3}$$

[33] At equilibrium, the driving forces are equal to the resisting forces. An increase in the driving forces or a decrease in the resisting forces will put the system out of equilibrium. This will result in a resultant force downslope and the consequent extension of the upslope slab (as for model 2) or the repeated failure of the headwall (as for model 1). Using equations (2) and (3) we are able to calculate the resultant force at different positions within the slab.

5.2.2. Initiation of Displacement

[34] According to static stability analyses carried out using our model, the factor of safety of the slope decreases if there is (1) a decrease in P; (2) an increase in u; (3) an increase in W_T; (4) an increase in γ; (5) an increase in S; (6) an increase in l; (7) an increase in θ; (8) a decrease in ϕ; and/or (9) a decrease in c. These results provide an insight into the potential triggers of a spread. Failure can be triggered by a temporal, rather than a spatial, change in one or many of the above variables. The variables that are more likely to undergo a temporal change are P, W_T and u. A spread can thus be initiated in a number of ways. A first trigger involves the loss of support at the foot of the slope, such as a slope failure occurring downslope of the spread and the consequent creation of a headwall. As noted in section 4.4, a steep escarpment or a slope failure scar is located at the distal part of most spreads within the Storegga Slide. A second trigger consists of an increase in W_T, which can be caused by loading of sediment from a slope failure occurring upslope of a spread. There are no indications that this process was responsible for triggering spreading within the Storegga Slide. However, we think that sediment redistribution and loading are potentially active during compression, and that these processes may reactivate sliding of blocks and the subsequent formation of windows within spreads. A third trigger of spreading can be an increase in pore pressure. This can be a result of contraction due to gas

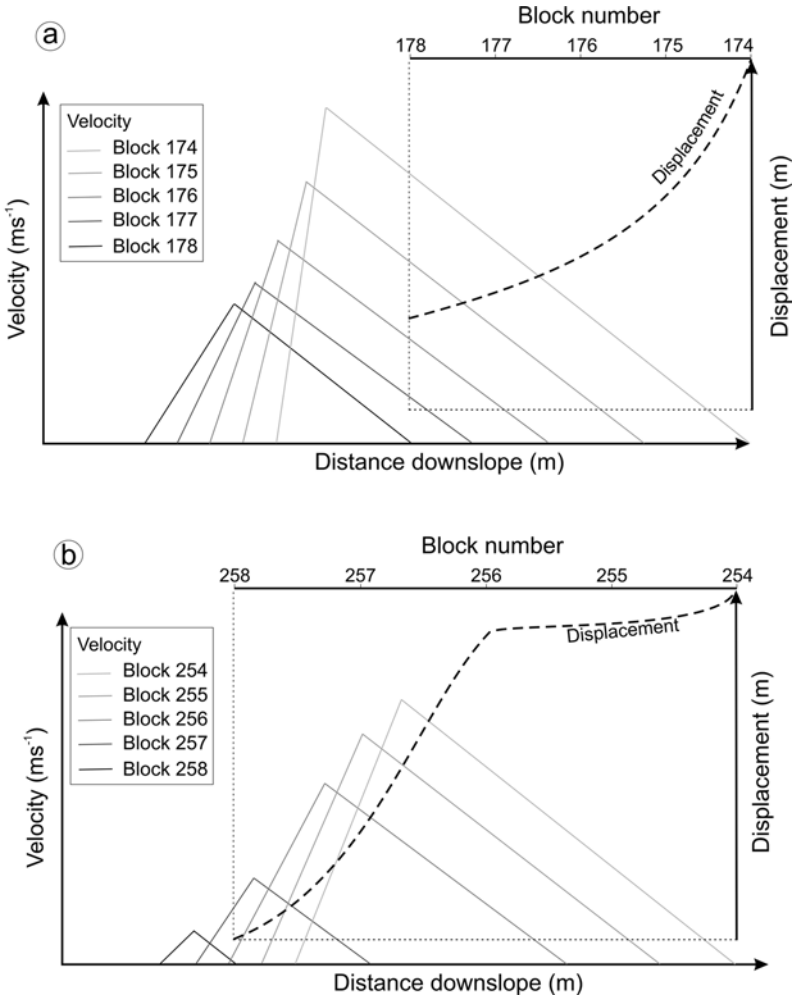

Figure 14. Plots of velocity versus distance downslope for a group of blocks in a theoretical spreading event modeled using values from the Storegga Slide in the mechanical model. The block numbers refer to the order in which a group of blocks in an upslope section of the slope is displaced. Also shown is the variation of block displacement with block number. (a) Block movement pattern observed in the middle of the slab. The resulting pattern is an exponential increase of displacement of blocks with distance downslope. (b) Block movement pattern for the upslope 1.5 km of the slab where an increase in angle of internal friction occurs because of an overconsolidated layer developed during the Last Glacial Maximum. The resulting pattern shows a steep decrease in displacement, which should coincide with the formation of a steep headwall.

hydrate dissociation or seismic loading. Gas hydrate dissociation is dismissed as a potential trigger because we found no evidence of bottom simulating reflectors in the seismic data from the spreading areas, and there are no signs of gas hydrates in geoborings from these areas [*Kvalstad et al.*, 2005a]. *Kvalstad et al.* [2005a] argue that seismic loading is an unlikely cause of spreading because it has to be of high magnitude and take place over very large areas simultaneously. The Møre Basin, where the Storegga Slide is located, is a deep sedimentary basin that is surrounded by large structures with harder rocks, such as the volcanic marginal high in the southwest, the Caledonian basement and prerift sediments in the east, and the Oligocene/Miocene sediments of the Helland-Hansen Arch in the north. In such a structural setting, the seismic energy is likely to become trapped and the influence of the earthquake prolonged, thus affecting large areas instantaneously [*Lindholm et al.*, 2005]. The source of such a seismic event could have been the glacial isostatic rebound of the Fennoscandian shield [*Atakan and Ojeda*, 2005]. Therefore we propose than an increase in pore pressure could have been induced by seismic loading. Seismic activity is itself a potential fourth trigger because it may have initiated spreading in two other ways. Seismic loading induces downslope shear stresses that can lead to short-term failure in the sediment. Glacial isostatic rebound, to which the seismic activity is associated, may result in both the sediment and the slip surface becoming steeper, which would also promote instability. Additionally, the combined effect of pore pressure buildup and seismic shear stresses may lead to plastification or liquefaction of the slip layer. Sediment samples taken from the weak layer can actually liquefy under sufficient dynamic loading [*Sultan et al.*, 2004a] and seismic data from the northern sidewall show

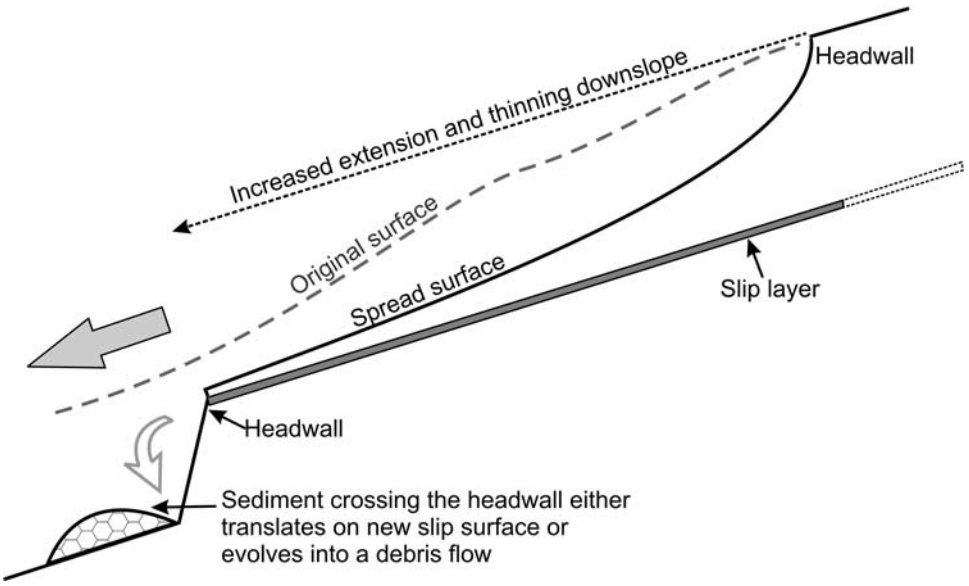

Figure 15. Schematic cross section through a typical spread within the Storegga Slide.

subsurface sediment disturbance that could be the result of liquefaction [*Berndt et al.*, 2003, 2004]. It is therefore possible that liquefaction controlled the properties of the slip layer for the spreading, particularly as this process of the slip layer is considered to be the main cause of spreading in subaerial environments [*Bartlett and Youd*, 1995]. If liquefaction is only possible for some sedimentary layers and not for most others, this would explain why the spreads occur consistently on the same slip surfaces. Seismic activity has also been identified as the most probable trigger of the entire Holocene Storegga Slide [*Bryn et al.*, 2005a]. On the basis of all the above considerations we conclude that loss of support and seismic loading are the most likely triggers of spreading within the Storegga Slide.

5.2.3. Mechanical Model

[35] Our model can also be used to constrain the behavior of the sediment blocks after slope failure has occurred. Assuming that shear planes are formed between the individual blocks in Figure 13, equations of motion were applied to each block separately. If we consider the failure as instantaneous, the resultant force, acceleration, velocity and distance traveled by each block can be calculated for different distances downslope from a fixed point upslope. Fluid resistance and friction at the base of the block are included in the mechanical model. They are assumed to be responsible for decelerating the blocks and are considered constant along the entire length of the slab. Initially, we also assume that the mass of a failed block does not change as it moves downslope. Although we study the movement of each block separately, in reality the blocks move as a group.

[36] This model was applied using values for the different variables from the Storegga Slide. These values were estimated from a 35 km long section of the seismic line NH0163-n102. The width of the blocks is 130 m (resulting in a total of 269 blocks) whereas the slope gradient of the slip surface (θ) changes from 1° at the headwall to 0.96° in the distal part (a decrease of 1.15° per 1000 km). Along the entire slab, the sediment thickness (S) is considered constant at 80 m (this corresponds to the thickest part of the failed sediment in Figure 10). The sediments in this region are thought to become more consolidated upslope toward the shelf edge because of compaction by glacial advance during glacial maxima. Therefore we use values of 9 kN m^{-2} for the unit weight (γ) and 25° for the angle of internal friction ($\varnothing$) at the downslope limit [*Kvalstad et al.*, 2005a], which increase linearly to 10 kN m^{-2} for γ and 27.5° for $\varnothing$ at the upslope limit (which is the slope gradient of the headwall at this point). An overconsolidated sediment layer that developed during the LGM is known to occur close to the main headwall [*Bryn et al.*, 2005a]. Thus, at 1.5 km from the upslope limit we increase γ linearly from 10 kN m^{-2} to 10.5 kN m^{-2} at the headwall. Unloading of the sediment after the LGM has reduced pore pressures in sediments close to the headwall, while measured pore pressures are higher near the North Sea Fan [*Bryn et al.*, 2003; *Strout and Tjelta*, 2005]. Pore pressure (u) is thus decreased from 1000 kN m^{-2} at the downslope limit to 600 kN m^{-2} at the upslope limit of the slab [*Strout and Tjelta*, 2005]. The cohesion (c) in this part of the Storegga Slide is spatially constant at 7 kN m^{-2} [*Sultan et al.*, 2004b]. The supporting force (P) prior to failure is determined for each block by balancing the driving and resisting forces.

[37] Since loss of support is the most likely trigger of spreading within the Storegga Slide, the spread in the mechanical model is triggered by the removal of the sediment at the distal part of the slope and reduction of P to 0 for block 1. The graph in Figure 14a shows the velocity attained and distance covered by blocks in the middle section of the slab. The first block to be released has the highest values of W_T, l and u, and the lowest values of γ, $\varnothing$ and θ. These conditions generate the highest possible resultant force, and therefore the highest velocity and longest distance covered. For successive blocks upslope, W_T, l, u, γ, $\varnothing$ and θ change, resulting in a lower resultant force, and thus lower velocities and shorter distances traveled (Figure 14a). The variation of the displacement

for each block is also shown. The curve illustrates that the displacement of the blocks increases exponentially with distance downslope. This pattern is similar to the empirically estimated ridge displacement pattern (Figure 12).

[38] The graph in Figure 14b shows the velocity attained and distance covered by blocks in the upslope 1.5 km of the slope, where a further increase in γ occurs. The abrupt decline in displacement of blocks 257 and 258 explains the spreading pattern observed near some sections of the main Storegga headwall, where the displacement of the extended ridges decreases rapidly upslope and a steep, stable headwall is formed (Figure 8c). Without the increase in γ upslope, we would expect the displacement of the blocks to decrease gradually upslope until a low and gentle headwall is formed (Figure 8d).

[39] In the above mechanical model we assumed that the failure was instantaneous. It is important to appreciate that the block displacement pattern illustrated in Figure 14 could also be the result of an increase in the duration of movement of successive blocks with distance downslope. The geophysical data does not provide any information to understand whether the increase in displacement with distance downslope is due to an increase in velocity alone, or due to an increase in both velocity and time (Figures 5 and 6).

[40] In our mechanical model we do not consider tilting, distortion, plastic deformation or loss of excess pore pressure due to block fragmentation. If these factors were to be taken into account, their combined effect would be to slow down the movement of the downslope blocks most, expending the kinetic energy and resulting in a subdued exponential decay (as observed in Figure 12).

[41] The distance traveled by the blocks in the distal part of the slope would theoretically increase continuously with the length of the slope. This is, of course, not the case, as we do observe that the distal parts of spreads stopped either on the slope or after crossing an escarpment. Apart from fluid friction and kinetic friction with the underlying sediments, other factors are involved in slowing down a spread. With increasing translation downslope, the distal part of the spread undergoes increasing fragmentation and remolding because of either friction or collapse over a headwall. This disintegration may allow escape of excess pore pressure from the base of the spread, reducing the resultant force acting on the spread and bringing it to a halt. Additionally, as the spread extends and breaks up, it is likely to become thinner. Such thinning can be observed in the seismic data (Figures 9a and 10a). The decrease in S, combined with the decrease in θ with distance downslope, will also reduce the resultant force acting on the spreading unit, retarding the block displacement further.

5.3. Development of Spreading Within the Storegga Slide

[42] We use the results from the previous calculations and models to describe how spreads develop within the Storegga Slide (Figure 15). The most probable trigger for spreads is either loss of support, due to mass movements occurring downslope of a potential spreading unit, or seismic loading, which results in pore pressure development and downslope shear stresses. A spread may thus initiate somewhere along its length, with the failure propagating upslope from this point, or it may initiate instantaneously over large portions of its area. Once a spread is triggered, the sediment unit breaks up into a number of blocks. The formation of the shear planes between the blocks obeys the Mohr-Coulomb failure criterion. A pattern of parallel to subparallel ridges and troughs forms at the surface. The ridges are orientated perpendicular to the direction of movement. The blocks at the leading edge of the spread are displaced the most. The distal end generally collapses over the preexisting downslope headwall created by the mass movement that triggered the spread, and the sediment either evolves into a debris flow or translates on a different slip surface, preserving the ridge and trough morphology. The seafloor located downslope of the headwalls in the distal part of zone 1 is characterized by a blocky morphology, whereas subtle ridge and trough morphology can still be observed in spreading material that has crossed the distal headwall in zone 2. This means that what happens to the material at the distal end of a spread depends on its sediment properties, in particular its consolidation and thickness.

[43] Spreading primarily involves extensional deformation. In some places, however, the spread may have undergone compression, as suggested by the presence of groups of high convex-downslope ridges and troughs (Figure 4a), and as previously described in other mass movements [e.g., *Lastras et al.*, 2006]. This compression is attributed to the slowing down of the leading edge because of, for example, increased fragmentation and the associated reduction in pore pressure, or a decrease in the gradient of the slip surface. Consequently, the ensuing blocks may collide with the immobilized blocks, resulting in overthrusting and compression. The morphological signature of compression is a series of ridges and troughs that tend to be longer and more pronounced than those formed by extension. During compression, the spreading layer may heave and become thicker. Where this occurs, the increased thickness in the sediment may reactivate mobilization in the form of translational mass movements.

[44] Extension, friction and water resistance, acting on the major part of the spread, fragment and remold the blocks as they move downslope. These result in the escape of excess pore pressure from the sediment and thinning of the failing unit, which slow and finally halt the mobilized sediment. Fragmentation of the blocks decreases upslope. The displacement of blocks decreases exponentially upslope until the driving and resisting forces reach equilibrium at the headwall. In reality, the block extension pattern may be more complex and involve different scales of fracturing. Figures 4b and 12 indicate that the sediment unit may initially break up into a number of relatively large blocks. Subsequently, each of these blocks fragments into a number of smaller blocks. The groups of small blocks exhibit an exponential decay of displacement upslope, in accordance with the general pattern displayed by all the blocks (Figure 12). A gradual decrease in the thickness of the spreading unit also accompanies the increasing displacement downslope (Figures 9a and 10). The overall extension of a sediment unit during spreading results in the lowering of the seabed. According to the observed pattern of block displacement, we would expect the spread to gradually transform into a stable slope as it extends upslope, forming a shallow and gentle headwall. This only occurs in zone 3, however, because the presence of overconsolidated sedi-

ment due to glacial compaction in zones 1 and 2 retards block displacement further and results in a higher and steeper headwall.

[45] As shown in section 5.2.3, the factors that vary the most across a sediment subunit are the angle of internal friction, pore pressure and the gravitationally induced stress, the latter being determined by the thickness of the sediment, the length of slope upslope and the unit weight. These three factors are thus considered the major controls of the extent of spreading and responsible for the exponential increase of block displacement with distance downslope. The decrease in the thickness of the O3 subunit upslope [*Berg et al.*, 2005] may also play a role in determining the position of the main headwall in zone 1. As shown in Figure 9b, the gradient of the slip surface mainly controls the direction in which a sediment unit spreads. This has also been observed in terrestrial spreading in Japan [*Youd and Kiehl*, 1996].

[46] There are two modes of spreading within the Storegga Slide. Within zone 1a the failing sediment behaves as a slab that is extended and breaks up into a number of blocks (model 2). The similarity in ridge and trough morphology indicates that zone 1b fails in the same way. Spreading within zones 2 and 3 occurs via the retrogressive unloading of the headwall, as explained by *Kvalstad et al.* [2005a] (model 1). The different behavior of zones 1 and 2 presumably reflects differences in sediment type. In zone 1, failure occurs in thin, stratified sediment with a high clay content (up to 65%), which enables it to behave as a thin slab undergoing extension along its entire length [*Berg et al.*, 2005]. The thicker sediment in zone 2 has lower clay content (up to 40%), and failure occurs along a distinct stratigraphic boundary. Zone 3, on the other hand, might represent a variation on zone 2 where the O3 sediment subunit, acting as the slip layer, is on the point of pinching out. Because of this, the extent of spreading upslope of the scarp is restricted. The failure of these sediments as a spread, rather than other types of mass movement, is attributed to the deep burial of the subunits O3 and O4–O7. These sediments are more compacted and thus favor brittle deformation, although the sediment in the distal part of the spread undergoes plastic deformation. The plastic deformation may be attributed to the higher deformation and the increasing pore pressure in the sediment with distance downslope [*Strout and Tjelta*, 2005]. Failure generally occurs in stratigraphically inhomogeneous sediments, which promote mass movement through basal deformation [*Laberg and Vorren*, 2000]. Spreading occurs along surfaces within the fine-grained contouritic sediments (O3 and R2 subunits), which are characterized by higher water content, clay content and plasticity, and lower unit weight with respect to the glacial sediments [*Kvalstad et al.*, 2005b]. The fine-grained sediments are thus more sensitive than the poorly sorted and coarser-grained glacial sediments [*Bryn et al.*, 2005b].

[47] The properties of the sediment unit in which spreading occurs also have a direct control on ridge and trough morphology. The ridges in zone 2 are the longest, the most widely spaced and they have the deepest troughs. The larger spacing can be explained by the greater burial depth and higher consolidation of the sediments, which results in a higher angle of internal friction and unit weight [*Berg et al.*, 2005]. The sediment failing in zone 2 is also the thickest. Overall these conditions generate a high gravitationally induced stress. This results in a higher acceleration of the blocks, as well as a steeper exponential decay in block displacement with distance downslope, which is reflected in higher ridge spacing. The latter also causes the troughs between the blocks to be deeper. The blocks are more consolidated and they do not break down as easily as blocks in the shallower sediments, resulting in longer ridges. As spreading occurs in progressively shallower, thinner and less consolidated units (zones 1a, 1b and 3), the ridges are observed to be shorter, more closely spaced and separated by shallower troughs (Table 1). The sediment also undergoes more plastic deformation.

6. Conclusions

[48] Spreading is a type of mass movement that has occurred over at least 25% of the Storegga Slide scar. It can be identified by a recurrent extensional pattern of parallel ridges and troughs, oriented perpendicular to the direction of mass movement and occurring at a variety of scales. Loss of support and seismic loading are the main triggering mechanisms. A spread develops by Mohr-Coulomb failure of a surficial sediment unit into coherent blocks that are displaced downslope along planar slip surfaces. Two modes of failure can be identified within the Storegga Slide: retrogressive failure of the headwall in the Ormen Lange region and above the northern sidewall, and slab extension and rupturing in the other spreading zones. The mode of failure seems to be determined by the clay content and thickness of the sediment in which spreading occurs, and the nature of the slip layer. The spreading process is mainly extensional, although localized events of compression also occur. Block movement patterns entail an exponential increase of displacement with distance downslope, which is accompanied by thinning of the failing sediment. The distal edge of the spread generally collapses over a headwall created by an earlier mass movement farther downslope. The extension of the remaining sediment gradually declines upslope until the spread is brought to a halt at the upslope limit, where a headwall is formed. The factors responsible for this sediment deceleration are one or many of the following: excess pore pressure escape due to fragmentation of the spreading sediments, reduction in gravitationally induced stress, increase in angle of internal friction of the sediment, decrease in the gradient of the slip surface and/or friction. The extension associated with spreading is on the order of 10%.

[49] Spreading within the Storegga Slide and other submarine slope failures has been largely overlooked because of the inability of acoustic data acquisition techniques to resolve its structure in sufficient detail. With modern high-resolution data sets it can now be demonstrated that spreading is a significant and widespread style of submarine mass movement worldwide. Spreads tend to occur over relatively large regions and on gently sloping terrain that superficially would appear stable. With huge investments currently being made in deepwater oil and gas exploitation worldwide, the hazard posed by submarine spreading needs to be recognized and understood. Movement associated with spreading is generally limited, in the range of hundreds of meters, but

is nevertheless sufficient to destroy seabed structures and disrupt pipelines.

Notation

Model for calculation of interblock displacement in a spread

- o distance between two reference points (here regarded as the top upslope corners of the two blocks) prior to failure, m
- n new distance between the two reference points after failure, m
- h sum of the vertical distances that the downslope corner of the upslope block and the upslope corner of the downslope block in the model have moved during failure, m
- α angle of anticlockwise tilting of a block, deg

Limit equilibrium model for a spread

- θ slope gradient of slip surface, deg
- W_T total weight of sediment upslope of a block = γSl, N
- γ submerged unit weight (in two dimensions), N m^{-2}
- S sediment unit thickness prior to failure, m
- l distance from a fixed point upslope, m
- $ø$ angle of internal friction, deg
- u pore water pressure (in two dimensions), N m^{-2}
- c cohesion, N m^{-2}
- P supporting force from slab downslope, N

[50] **Acknowledgments.** This research was supported by the HERMES project, EC contract GOCE-CT-2005-511234, funded by the European Commission's Sixth Framework Programme under the priority "Sustainable Development, Global Change and Ecosystems." We would like to thank Norsk Hydro AS for providing the bathymetric data and the high-resolution 2-D seismic lines. BP Norway and the European North Atlantic Margin (ENAM) II Programme are acknowledged for making available the 3-D seismic data set and TOBI side-scan sonar imagery, respectively. We are grateful to Michael Church, Tim Davies, Galderic Lastras, and Mauri McSaveney for their insightful reviews.

References

Atakan, K., and A. Ojeda (2005), Stress transfer in the Storegga area, offshore mid-Norway, *Mar. Pet. Geol.*, *22*, 161–170.

Bartlett, S. F., and T. L. Youd (1995), Empirical prediction of liquefaction-induced lateral spread, *J. Geotech. Eng.*, *121*, 316–329.

Berg, K., A. Solheim, and P. Bryn (2005), The Pleistocene to recent geological development of the Ormen Lange area, *Mar. Pet. Geol.*, *22*, 45–56.

Berndt, C., S. Bünz, and J. Mienert (2003), Polygonal fault systems on the mid-Norwegian margin: A long term source for fluid flow, in *Subsurface Sediment Mobilization*, edited by P. van Rensbergen et al., *Geol. Soc. Spec. Publ.*, *216*, 283–290.

Berndt, C., J. Mienert, M. Vanneste, and S. Bünz (2004), Gas hydrate dissociation and seafloor collapse in the wake of the Storegga Slide, Norway, in *Onshore-Offshore Relationships on the North Atlantic Margin*, *Norw. Pet. Soc. (NPF) Spec. Publ.*, vol. 12, edited by B. T. G. Wandås et al., pp. 285–292, Elsevier, Amsterdam.

Bryn, P., A. Solheim, K. Berg, R. Lein, C. F. Forsberg, H. Haflidason, D. Ottesen, and L. Rise (2003), The Storegga Slide complex: Repeated large scale sliding in response to climatic cyclicity, in *Submarine Mass Movements and Their Consequences*, edited by J. Locat and J. Mienert, pp. 215–222, Kluwer Acad., Dordrecht, Netherlands.

Bryn, P., K. Berg, C. F. Forberg, A. Solheim, and T. J. Kvalstad (2005a), Explaining the Storegga Slide, *Mar. Pet. Geol.*, *22*, 11–19.

Bryn, P., K. Berg, M. S. Stoker, H. Haflidason, and A. Solheim (2005b), Contourites and their relevance for mass wasting along the Mid-Norwegian margin, *Mar. Pet. Geol.*, *22*, 85–96.

Buma, J., and T. van Asch (1996), Soil (debris) spreading, in *Landslide Recognition: Identification, Movement and Courses*, edited by R. Dikau et al., pp. 137–148, John Wiley, Chichester, U.K.

Canals, M., et al. (2004), Slope failure dynamics and impacts from seafloor and shallow sub-seafloor geophysical data: Case studies from the COSTA project, *Mar. Geol.*, *213*, 9–72.

Dikau, R., D. Brunsden, L. Schrott, and M. L. Ibsen (Eds.) (1996), *Landslide Recognition: Identification, Movement and Causes*, John Wiley, Chichester, U.K.

Dobry, R., and M. H. Baziar (1992), Modeling of lateral spreads in silty sands by sliding soil blocks, paper presented at Speciality Conference on Stability and Performance of Slopes and Embankments, Am. Soc. of Civ. Eng., Berkeley, Calif.

Evans, D., et al. (2005), Palaeoslides and other mass failures of Pliocene to Pleistocene age along the glaciated European margin, *Mar. Pet. Geol.*, *22*, 1131–1148.

Gauer, P., T. J. Kvalstad, C. F. Forsberg, P. Bryn, and K. Berg (2005), The last phase of the Storegga Slide: Simulation of retrogressive slide dynamics and comparison with slide-scar morphology, *Mar. Pet. Geol.*, *22*, 171–178.

Haflidason, H., H. P. Sejrup, A. Nygård, P. Bryn, R. Lien, C. F. Forsberg, K. Berg, and D. G. Masson (2004), The Storegga Slide: Architecture, geometry and slide development, *Mar. Geol.*, *231*, 201–234.

Haflidason, H., R. Lien, H. P. Sejrup, C. F. Forsberg, and P. Bryn (2005), The dating and morphometry of the Storegga Slide, *Mar. Pet. Geol.*, *22*, 123–136.

Kanibir, A., R. Ulusay, and O. Aydan (2006), Assessment of liquefaction and lateral spreading on the shore of Lake Sapanca during the Kocaeli (Turkey) earthquake, *Eng. Geol.*, *83*, 307–331.

Krastel, S., R. B. Wynn, T. J. J. Hanebuth, R. Henrich, C. Holz, H. Meggers, H. Kulhmann, A. Georgiopoulou, and H. D. Schulz (2006), Mapping of seabed morphology and shallow sediment structure of the Mauritania continental margin, North-west Africa: Some implications for geohazard potential, *Norw. J. Geol.*, *86*, 163–176.

Kvalstad, T. J., L. Andersen, C. F. Forsberg, K. Berg, P. Bryn, and M. Wangen (2005a), The Storegga Slide: Evaluation of triggering sources and slide mechanisms, *Mar. Pet. Geol.*, *22*, 245–256.

Kvalstad, T. J., F. Nadim, A. M. Kaynia, K. H. Mokkelbost, and P. Bryn (2005b), Soil conditions and slope stability in the Ormen Lange area, *Mar. Pet. Geol.*, *22*, 299–310.

Laberg, J. S., and T. O. Vorren (2000), The Trænadjupet Slide, offshore Norway—Morphology, evacuation and triggering mechanisms, *Mar. Geol.*, *171*, 95–114.

Laberg, J. S., T. O. Vorren, J. Mienert, D. Evans, B. Lindberg, D. Ottesen, N. H. Kenyon, and S. Henriksen (2002), Late Quaternary palaeoenvironment and chronology in the Trænadjupet Slide area offshore Norway, *Mar. Geol.*, *188*, 35–60.

Lastras, G., M. Canals, and R. Urgeles (2003), Lessons from sea-floor and subsea-floor imagery of the BIG'95 debris flow scar and deposit, in *Submarine Mass Movements and Their Consequences*, edited by J. Locat and J. Mienert, pp. 425–431, Kluwer Acad., Dordrecht, Netherlands.

Lastras, G., M. Canals, D. Amblas, M. Ivanov, B. Dennielou, L. Droz, A. Akhmetzhanov, and TTR-14 Leg 3 Shipboard Scientific Party (2006), Eivissa slides, western Mediterranean sea: Morphology and processes, *Geo Mar. Lett.*, *26*, 225–233.

Lindberg, B., J. S. Laberg, and T. O. Vorren (2004), The Nyk Slide—Morphology, progression, and age of a partly buried submarine slide offshore northern Norway, *Mar. Geol.*, *213*, 277–289.

Lindholm, C., M. Roth, H. Bungum, and J. I. Faleide (2005), Probabilistic and deterministic seismic hazard results and influence of the sedimentary Møre Basin, NE Atlantic, *Mar. Pet. Geol.*, *22*, 149–160.

Marrett, R., and R. W. Allmendinger (1992), Amount of extension on "small" faults: An example from the Viking graben, *Geology*, *20*, 47–50.

Micallef, A., C. Berndt, D. G. Masson, and D. A. V. Stow (2007), A technique for the morphological characterization of submarine landscapes as exemplified by debris flows of the Storegga Slide, *J. Geophys. Res.*, *112*, F02001, doi:10.1029/2006JF000505.

Mulder, R., and P. Cochonat (1996), Classification of offshore mass movements, *J. Sediment. Res.*, *66*, 43–57.

Piper, D. J. W., P. Cochonat, and M. L. Morrison (1999), The sequence of events around the epicentre of the 1929 Grand Banks earthquake: Initiation of debris flows and turbidity currents inferred from sidescan sonar, *Sedimentology*, *46*, 79–97.

Solheim, A., K. Berg, C. F. Forsberg, and P. Bryn (2005), The Storegga Slide complex: Repetitive large scale sliding with similar cause and development, *Mar. Pet. Geol.*, *22*, 97–107.

Strout, J. M., and T. I. Tjelta (2005), In situ pore pressures: What is their significance and how can they be reliably measured?, *Mar. Pet. Geol.*, *22*, 275–285.

Sultan, N., et al. (2004a), Triggering mechanisms of slope instability processes and sediment failures on continental margins: A geotechnical approach, *Mar. Geol.*, *213*, 291–321.

Sultan, N., P. Cochonat, J. P. Foucher, and J. Mienert (2004b), Effect of gas hydrates melting on seafloor slope instability, *Mar. Geol.*, *213*, 379–401.

Terzaghi, K., and R. B. Peck (1967), *Soil Mechanics in Engineering Practice*, 2nd ed., John Wiley, New York.

Vanneste, M., J. Mienert, and S. Bünz (2006), The Hinlopen Slide: A giant, submarine slope failure on the northern Svalbard margin, Arctic Ocean, *Earth Planet. Sci. Lett.*, *245*, 373–388.

Varnes, D. J. (1978), Slope movement types and processes, in *Landslides—Analysis and Control*, *Spec. Rep. 176*, 11–33 pp, Transp. Res. Board, Natl. Acad. of Sci., Washington, D. C.

Youd, T. L., and S. J. Kiehl (1996), Distribution of ground displacements and strains induced by lateral spread during the 1964 Niigata earthquake, in *Proceedings From the 6th Japan-U.S. Workshop on Earthquake Resistant Design of Lifeline Facilities and Countermeasures Against Soil Liquefaction*, edited by M. Hamada and T. D. O'Rourke, *Rep. NCEER-96-0012*, pp. 205–219, Multidiscip. Cent. for Earthquake Eng. Res., Buffalo, N. Y.

Youd, T. L., C. M. Hansen, and S. F. Bartlett (2002), Revised multilinear regression equations for prediction of lateral spread displacement, *J. Geotech. Geoenviron. Eng.*, *128*, 1007–1017.

C. Berndt, D. G. Masson, A. Micallef, and D. A. V. Stow, National Oceanography Centre, European Way, Southampton SO14 3ZH, UK. (amicall@noc.soton.ac.uk)